Auxiliary subunits keep AMPA receptors compact during activation and desensitization

Jelena Baranovic and Andrew J.R. Plested[§]

Institute of Biology, Cellular Biophysics, Humboldt Universität zu Berlin, 10115 Berlin; Leibniz Forschungsinstitut für Molekulare Pharmakologie (FMP), 13125 Berlin; NeuroCure, Charité Universitätsmedizin, 10117 Berlin, Germany.

[§]To whom correspondence should be addressed: plested@fmp-berlin.de

Summary

Signal transduction at vertebrate excitatory synapses involves the activity of ionotropic glutamate receptors, including the AMPA (α-amino-3-hydroxy-5-methyl-4-isoaxazole propionate) receptor. Technical advances in cryo-electron microscopy have brought a slew of full-length structures of AMPA receptors, on their own and in combination with auxiliary subunits. These structures illustrate a wide range of conformations, indicating that individual domains might undergo substantial lateral and rotational motions during gating. Here, we used bifunctional methanethiosulfonate cross-linkers to calibrate the conformations that occur in functional AMPA receptors both in the presence and absence of the auxiliary subunit Stargazin. Our data indicate that receptors without auxiliary subunits have considerably more conformational freedom and can get trapped in relaxed conformations. In contrast, Stargazin maintains both activated and desensitized receptors in compact arrangements. Thus, auxiliary subunits not only change the kinetics and trafficking of receptors, but also restrict their structural dynamics.

Introduction

AMPA-type glutamate receptors are found at excitatory synapses throughout the mammalian brain, where they convert glutamate release into membrane depolarisation. Their fast kinetics (Colquhoun et al., 1992; Geiger et al., 1995; Taschenberger and von Gersdorff, 2000), as well as the physical attributes of synapses(Xu-Friedman and Regehr, 2003), allow them to follow glutamate transients at rates above 100 Hz. However, the structural dynamics underlying their rapid signalling are unclear. AMPA receptors are tetrameric ligand-gated ion channels with unique architectural features and loosely coupled structural domains: unstructured linkers connect the amino- and ligand-binding domains (ATDs and LBDs, respectively) forming the extracellular part of the receptor. The LBDs are in turn connected to the transmembrane region (TM) that harbors the integral ion channel (Fig. 1A). The extracellular domains adopt local dimer pairs in resting and active receptors. The LBD dimers 'break up' in the desensitized state (Sun et al., 2002; Armstrong et al., 2006; Dürr et al., 2014; Twomey et al., 2017b), but motions of the ATDs (if any) are unclear (Herguedas et al., 2016; Cais et al., 2014; Yelshanskaya et al., 2016).

The crowded and narrow synaptic cleft is scarcely wider than the receptors are tall themselves and has narrow edges (Zuber et al., 2005; Tao et al., 2018). This observation implies that conformational dynamics of the receptor domains and their relation to synapse dimensions and molecular composition has implications in both health and disease. For example, if extremely dilated conformations of AMPA receptors can be adopted rapidly, that is on the millisecond timescale of fast excitatory transmission, this could impact receptor anchoring at synapses. Activity-dependent anchoring might be a way to regulate synaptic strength (Constals et al., 2015). On the other hand, slow rearrangements could be relevant for trafficking, and in disease states.

Advances in the structural biology of ionotropic glutamate receptors (iGluRs) have produced a catalogue of static conformational snapshots. Very similar structures have been obtained in conditions corresponding to nominally very

different functional states (Chen et al., 2014; Dürr et al., 2014; Yelshanskaya et al., 2014). In addition, several structures suggest substantial movements of the extracellular domains when bound by agonist (Nakagawa et al., 2005; Dürr et al., 2014; Meyerson et al., 2014). In these structures, the domains “fall apart”, either breaking local symmetry states, adopting higher order symmetries or switching into a ring-like arrangement (Fig. 1A). This broad and confusing range of conformations makes ordering of these pictures according to the putative activation states (resting, open and desensitized) difficult. We therefore set out to investigate the conformational range of agonist bound AMPA receptors with the aim of distinguishing frequently-visited, short-lived conformations from the long-lived ones that likely have less direct relevance to synaptic transmission.

Previously, we demonstrated disulfide bonds and metal bridges trapping receptors in compact arrangements (Salazar et al., 2017; Baranovic et al., 2016; Lau et al., 2013). To measure the separation of domains, in this work we used bifunctional methanethiosulfonate cross-linkers (bis-MTS) of defined lengths (Loo and Clarke, 2001; Guan et al., 2002; Armstrong et al., 2006; Tajima et al., 2016) (Fig. 1D). These cross-linkers show specific combination with two free thiol groups, provided by engineered cysteine residues. The reactivity of these probes can in principle report distances, giving them the property of nanometre-scale molecular rulers.

Overall, our results suggest that the more dilated conformation of the receptor, the slower it is to access, but once attained, these conformations are stable. However, auxiliary subunits restrict the conformational ensemble, maintaining more compact arrangements. This kinetic classification suggests AMPA receptors at synapses have similar, compact geometries regardless of their instantaneous gating state.

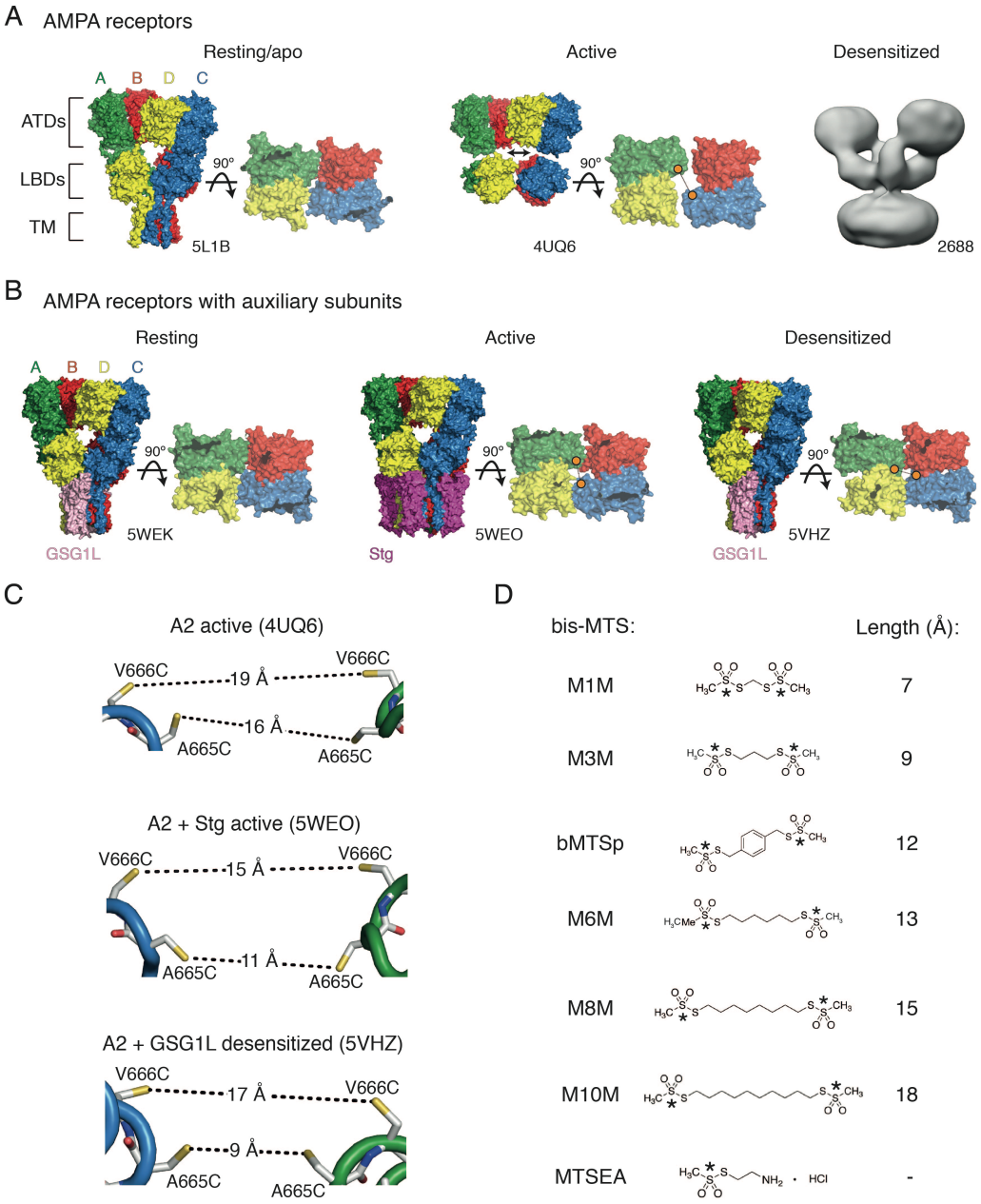

Figure 1 Geometry of AMPA receptors. (A) Structural models of full-length AMPA receptors in resting, active and desensitized states. Accesion codes for PBD or EMDB are indicated. Subunits are colour-coded: A – green, B – red, C – blue and D – yellow. Square brackets delineate AMPA receptor domains: ATDs – amino terminal domains, LBDs – ligand binding domains and TM – transmembrane domain. The cytoplasmic domain is not resolved. For the resting and active structures, LBDs are also shown in a top-down view (omitted for the desensitized structure due to its low resolution). Orange spheres connected by black lines indicate 665-666 residues (mutated in this study) in the LBD layer. (B) Same as in (A), but for A2 structures complexed with auxiliary subunits: Stg – Stargazin (dark purple) and GSG1L (light purple). (C) Distances between sulfhydryl groups of mutated residues, A665C and V666C, in agonist-bound strucures shown in (A) and (B). (D) Structures of bifunctional (bis-MTS: M1M-M10M) and monofunctional (MTSEA) compounds. Lengths were measured between reactive sulphur atoms (asterisks).

Results

Desensitized AMPA receptors can adopt 'relaxed' conformations

The rupture of the LBD intra-dimer interface is a structural hallmark of AMPA receptor desensitization, as shown by biophysical studies based on the structures of isolated dimers of ligand binding domains (Sun et al., 2002; Armstrong et al., 2006). Some cryo-electron microscopy (cryo-EM) structures of full-length receptors suggest that desensitization might involve further rearrangements of the ligand-binding domains, including separation of the two dimers and 'dilation' of the entire extracellular layer (Fig. 1A).

We attempted to capture this movement between LBDs with bis-MTS cross-linkers ranging from 7 to 18 Å in length (Fig. 1D). If the LBD layer opened up upon receptor desensitization, this movement should create access for the bis-MTS cross-linkers into the inter-dimer space of the LBD layer (orange dots in Fig. 1A).

We identified positions 665 and 666 (in the FG loop) in homomeric GluA2 receptors as best positioned to follow separation of the LBD dimers (Fig. 1A-C). The presumptive geometries of the sulfhydryl groups for cysteine mutants at these sites, in the agonist bound states of GluA2 receptor (with and without auxiliary subunits) are shown in Fig. 1C. The structure of the desensitized GluA2 receptor (EMDB: 2688, Fig. 1A) is not detailed enough to measure residue distances, but the equivalent residues are 21 Å apart in homologous kainate receptors (PDB: 5KUF; (Meyerson et al., 2016)).

As shown in Fig. 2B and D, bis-MTS cross-linkers M1M to M10M all caused strong reduction of the peak current in V666C mutant when applied in the desensitized state. To quantify this effect, the peak current was measured from the control pulses before (I_{peak} pre-trap, 4 pulses) and after the 1-minute application (trap) of the cross-linker (I_{peak} post-trap, 2nd control pulse after the trap, arrows in Fig. 2A-C). For each patch, the ratio of I_{peak} post-trap over I_{peak} pre-trap was determined and plotted as shown in Fig. 2D-E.

For the V666C mutant, bis-MTS cross-linkers from 7 to 15 Å in length (M1M-M8M; 1 μM), inhibited about 90% of the peak current in the patch after a 1 minute application (see Suppl. Table 1). The longest (M10M) cross-linker was the slowest one to act (Fig. 2F), leading to slightly less inhibition (~70%) in the first minute of exposure. The reduction was less pronounced for A665C mutant for all cross-linkers (~50%, Fig. 2E and Suppl. Table 1).

Inhibition was overall so profound that we sought to establish that it was specific. Two other factors potentially contribute to the current decrease: non-specific run-down of the current and disulfide bonding of the introduced cysteines to each other. Current run-down is particularly difficult to avoid in the long records that we made for these experiments. A665C and V666C sulfhydryl groups were both previously shown to crosslink in the presence of oxidizing agent CuPhen (Salazar et al., 2017; Lau et al., 2013; Yelshanskaya et al., 2016). To account for these confounding factors, we made paired recordings: a patch was first exposed to a 1-minute long trapping pulse containing glutamate only (no cross-linkers), followed by trapping of the same patch in glutamate and a cross-linker (Fig. 2B-C). Any run-down in the patch or possible cross-linking of the cysteines to each other was then assessed from trapping in glutamate only. Both mutants underwent some peak current reduction in glutamate in the absence of cross-linker (A665C: 0.78 $\pm$ 0.03, n = 23, $P <$ 0.0000001 vs. WT, V666C: 0.85 $\pm$ 0.02, n = 44, P = 0.003 vs. WT; WT A2: 0.97 $\pm$ 0.03, n = 30), consistent with previous results (Lau et al., 2013; Yelshanskaya et al., 2016) . Limited cross-linking of A665C cysteines to each other in long exposures to 10 mM glutamate was evident as a recovery of peak responses after the trapping pulse (grey dots in Fig. 2C, τ = 3.3 $\pm$ 0.4 s, n = 17). For the V666C mutant, all 6 bis-MTS cross-linkers (M1M-M10) resulted in substantially more current inhibition than glutamate alone ($P \leq 0.03$ with and without bis-MTS, depending on the cross-linker; paired randomisation test). Overall, paired recordings gave indistinguishable results to the non-paired recordings. In other

166 words, disulfide crosslinking and rundown were minimal in these conditions.
167 Therefore, we pooled these data (Fig. 2D-E).
168
169 To confirm that the observed peak current reduction came from crosslinking
170 rather than monofunctional engagement of a cross-linker, we modified mutants
171 with MTSEA (Fig. 1D), which can interact only with a single cysteine. As shown
172 in Fig. 2D-E, MTSEA failed to inhibit either V666C or A665C above control (I_{peak}
173 post-trap / I_{peak} pre-trap for V666C: 0.89 $\pm$ 0.025, n = 3-4, P = 0.1; for A665C:
174 0.81 $\pm$ 0.06, n = 3-4, P = 0.8). This result also suggests that the mild oxidizing
175 environment created by MTS compounds at 1μM has little tendency to promote
176 disulfide bond formation. Thus, bifunctional MTS cross-linking was necessary
177 for the peak current reduction observed in desensitizing AMPA receptors.
178
179 The effect of all bis-MTS cross-linkers with respect to their length is summarized
180 in the trapping profile for desensitized V666C receptors (Fig. 2G). Rather than
181 showing a preferred cross-linking length (and thus, conformation) for
182 desensitized receptors, the profile is a shallow parabola with strong effects
183 across all tested lengths. These results demonstrate that desensitized AMPA
184 receptors can 'open up' their LBD layer to at least 18 Å at position 666 during
185 desensitization, but occupy a spectrum of conformations. Structural
186 heterogeneity and 'dilation' of the LBD layer to ≥18 Å are both in good
187 agreement with cryo-EM structures (Meyerson et al., 2014; Dürr et al., 2014).

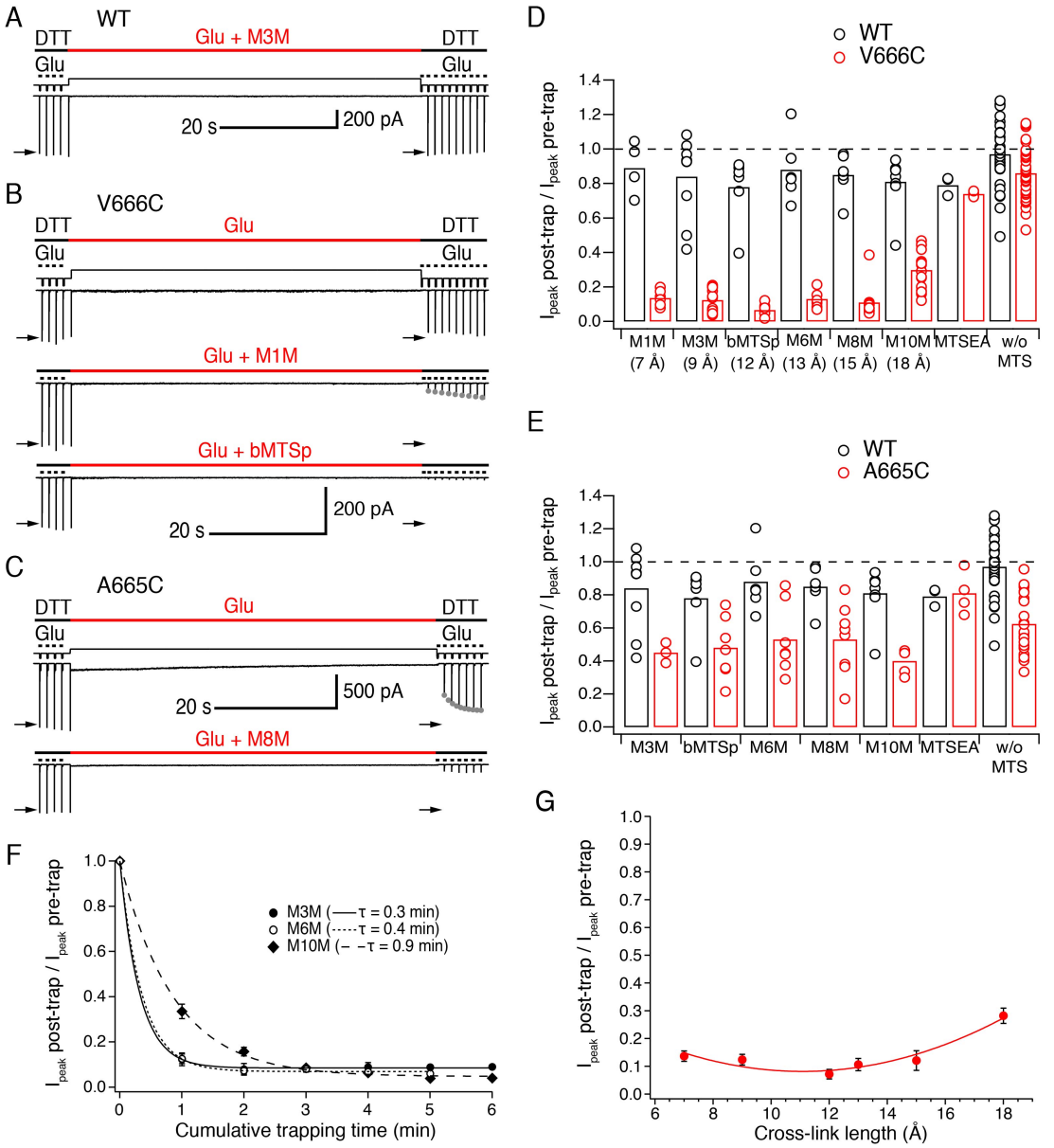

Figure 2 LBDs separate at least 18 Å in desensitized GluA2. (A) Control recording of wild-type (WT) GluA2 AMPA receptors in response to a trapping protocol. Movements of the piezo reflecting the solution exchange are shown in thin, black lines above the current trace. Composition of the solutions is indicated in thick lines above the piezo trace. Downward ticks are 200 ms control jumps from DTT (1 mM) to DTT and glutamate (Glu, 10 mM). Four pre-trap control pulses were followed by a 1-minute long trapping pulse (red line) in Glu (10 mM) and M3M (1 μM). After the trapping pulse, the patch was exposed to 10 post-trap control pulses. The first post-trap pulse gives no response because receptors are desensitized (for details, see Experimental Procedures). (B) Same as in (A), but for V666C mutant. The top two recordings are from the same patch: in the first trace, V666C receptors were exposed only to Glu. Trapping of the same patch in Glu and M1M (1 μM), results in pronounced peak current reduction, which partly recovered with $\tau_{recovery}$ = 30 ± 7 s, n = 5 (grey dots; post-trap control pulses extended to 30 for fit). The bottom trace is a different patch trapped in bMTSp (1 μM), showing even stronger peak current reduction without any recovery. (C) As in (B) but for the A665C mutant. The two traces are paired recordings of the same patch. Post-trap control pulses show that A665C does cross-link to itself, but most of the current recovers within

203 several seconds after the trap (grey dots; $\tau_{recovery}$ = 3.3 ± 0.4 s, n = 17). If the same patch is now trapped
204 in Glu and M8M (1 μM), the peak current reduction is much more pronounced and does not recover. (D)
205 Summary of the trapping effects for WT (black) and V666C (red) for cross-linkers M1M (7 Å) to M10M (18
206 Å). Trapping effect was calculated as the ratio of the post-trap and pre-trap peak current (arrows in A-C).
207 MTSEA is a monofunctional reagent and "w/o MTS" stands for "without MTS" (traps in Glu only, pooled
208 for all experiments). Dashed line indicates no effect. For peak current reduction in a bis-MTS vs. w/o MTS
209 (pooled), $P < 0.0000001$, for all cross-linkers. (E) Same as in (D), but for A665C (red) in cross-linkers
210 M3M (9 Å) to M10M (18 Å). A665C mutant in the presence and absence of an MTS cross-linker resulted
211 in $P \leq 0.02$, depending on the cross-linker. For statistics vs. WT, see Suppl. Table 1. (F) Trapping time for
212 V666C receptors in M3M, M6M and M10M. The 1-min trapping protocol was repeated up to 6 times,
213 resulting in a cumulative exposure of the patch to a bis-MTS of up to 6 min. The data were fit with a
214 monoexponential for each cross-linker (τ indicated in brackets). (G) Trapping profile of desensitized
215 V666C receptors shows the effect of each cross-linker vs. its length, in the first minute of exposure. The
216 data were fit with a parabola (red line): $f(x) = K_0 + K_1*(x - K_2)^2$ (for details, see Experimental Procedures).

217
218 In addition to positions 665 and 666, we also tested nearby positions 662 and
219 664 for their sensitivity to bis-MTS cross-linkers (Suppl. Fig. 1A). The I664C
220 mutant showed similar levels of the peak current reduction to V666C (Suppl.
221 Fig. 1B-C). However, we judged the I664C sulfhydryls were too far apart to
222 make effective use of the range of the available bis-MTS cross-linkers. Like the
223 A665C mutant, the S662C mutant showed considerable disulfide formation, so
224 we focused on the V666C mutant in further investigations.

225
226 Next, we wanted to test how specific the cross-linkers were in targeting the
227 inter-dimer interface of the LBD layer in our conditions. We generated another
228 single cysteine mutant, K493C (Armstrong et al., 2006), positioned within LBD
229 dimers (Suppl. Fig. 2A). Thus, bridging across the two cysteines should keep
230 the LBD dimers intact leading to block of desensitization. When we applied bis-
231 MTS cross-linkers on K493C receptors (1 μM, for ≥1 min), the effects were
232 profoundly different from the mutants at the inter-dimer interface: K493C
233 current underwent potentiation rather than inhibition, with shorter cross-linkers
234 (M1M, M3M and M6M) blocking the receptor desensitization almost completely
235 (Suppl. Fig. 2B-D). We also considered the possibility that bis-MTS cross-
236 linkers might be spuriously cross-linking to wild-type cysteines on the receptor
237 or forming inter-receptor cross-links (Suppl. Fig. 3A). If this were the case, the

238 peak current reduction effect would be expected to scale with the number of
239 the receptors in the membrane (i.e. peak current), but no such correlation was
240 found (Suppl. Fig. 3B). In addition, longer cross-linkers would be expected to
241 be more efficient in forging inter-receptor cross-links, but we found that the
242 longest cross-linker, M10M, was the slowest to react on desensitized AMPA
243 receptors (Fig. 2F). The absence of the strong peak current reduction in the WT
244 receptors also speaks against the bis-MTS cross-linkers interacting with native
245 cysteine residues. These results led us to conclude that the bis-MTS cross-
246 linkers are cross-linking cysteines introduced at the LBD inter-dimer interface
247 (V666C).
248
249 **Cross-linked desensitized states are highly stable**
250 Upon establishing specific and strong reduction of the peak current in
251 desensitizing V666C receptors by the bis-MTS cross-linkers, we next sought to
252 examine the stability of trapped states. The more stable the trapped state, the
253 longer we would expect that it takes for trapping effects to reverse, and vice
254 versa. The fastest recovery after trapping was observed with M1M (τ = 30 $\pm$
255 7 s, n = 5) and the time constant of the peak current recovery could be
256 measured by directly fitting the peak current of the post-trap control pulses (grey
257 dots in Fig. 2B). With longer bis-MTS cross-linkers, the recovery time increased
258 to minutes, making direct measurements of the recovery time from post-trap
259 control pulses impractical. Instead, the experimental design was adjusted to
260 allow measurements of long recovery times as described in Experimental
261 Procedures and Fig. 3. After the receptors were trapped with M3M for 1 minute,
262 the peak current in the patch did recover, but very slowly, taking over 10
263 minutes (600 applications of glutamate) to reach the pre-trapping levels. With
264 longer cross-linkers, the peak current was essentially irreversible over the
265 timescales we could measure (20 minutes; Fig. 3D-G). The progressive inability
266 of the receptors to recover from trapping with longer cross-linkers indicates
267 increasingly stable trapped states corresponding to greater separation of the A
268 and C subunits in the desensitized state (Fig. 3G-H). Desensitized AMPA

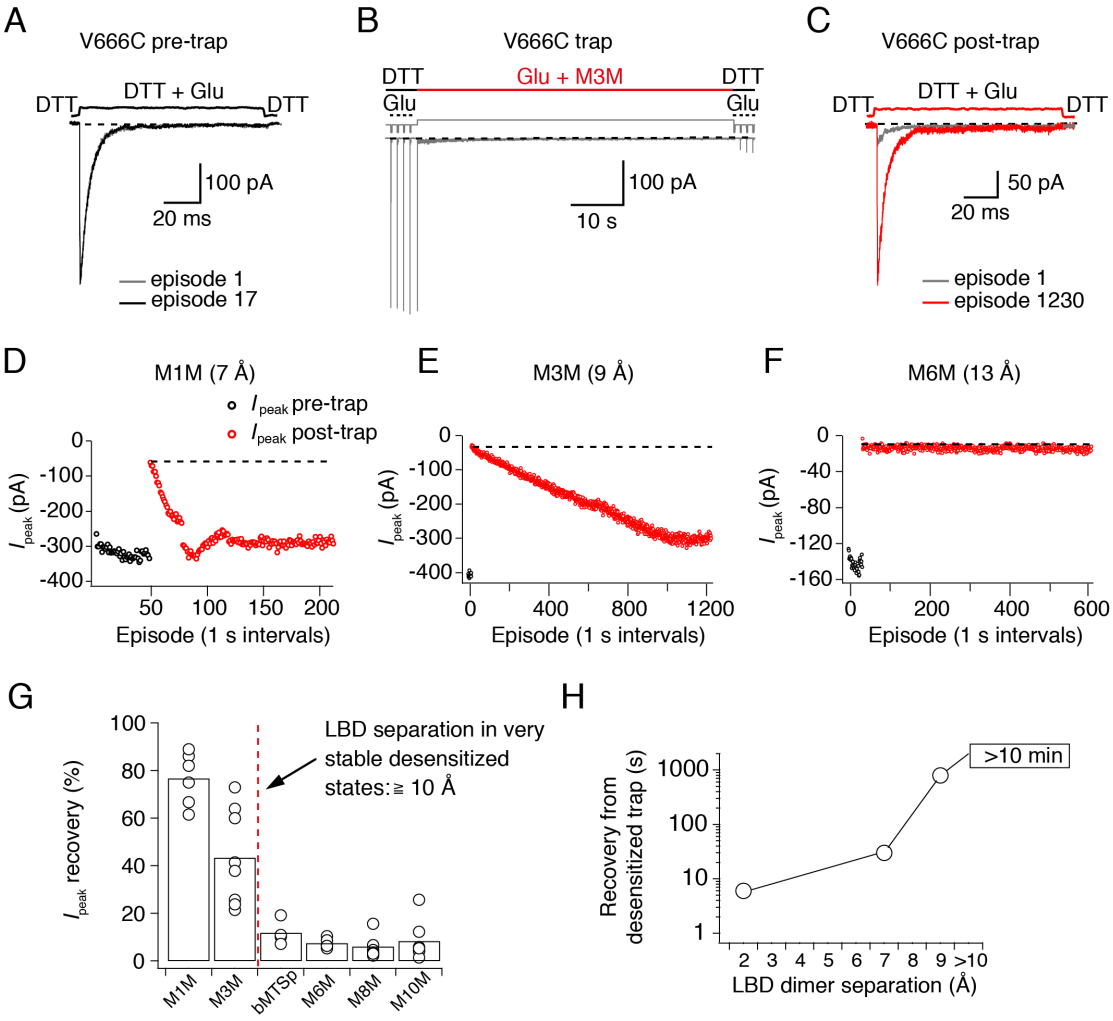

Figure 3 Recovery of trapped desensitized V666C receptors depends on the LBD separation. (A) Protocol to measure recovery from trapping. To obtain a stable baseline response to glutamate, we first repeated brief glutamate applications in reducing conditions (1 mM DTT). In the given example, we gave 17 pulses (100 ms, 1 Hz). (B) In the following step, the patch was exposed to 1 μM cross-linker (here M3M) and 10 mM Glu for 1 minute, with control pulses before and after the trap. (C) After the trapping protocol, the patch was again exposed to fast, reducing glutamate jumps like in (A) in order to follow recovery of the response. In this example, we could record 1230 consecutive episodes (~20 min) and obtain almost complete recovery. Note the difference between the current amplitude in the 1st episode (grey) and the 1230th episode (red). The recovery of the patch current (I_{peak}) in typical experiments for different cross-linkers is plotted in panels D - F (panel E is the same patch as panels A - C). Black dots show the response before the trap and red dots the peak current after the trap. The gap in red dots in (D) represents a switch between recording protocols. (G) Summary of the peak current recovery for different cross-linkers. The percentage of recovered current is the ratio of the peak currents recorded ~10 min after the trap to the peak current before trapping. Dashed red line denotes a limit after which no recovery of the current could be measured within 10 min after the trap. (H) Plot of recovery time from trapped desensitized states vs. the inter-dimer separation at position V666C in the LBD layer. The first data point indicates recovery from V666C disulphide bridges formed in desensitized state (Plested and Salazar, unpublished data).

288 receptors with a disulphide bridge formed between the two V666C residues at
289 inter-dimer interface fit in well with this trend, recovering in seconds following
290 100 s exposure to the oxidizing agent CuPhen (A.P. and Hector Salazar,
291 unpublished data) (Fig. 3H).
292
293 **Activation limits conformational heterogeneity of the LBD layer**
294 We next investigated if the LBDs of activated V666C receptors are also
295 accessible to a similarly wide range of bis-MTS cross-linkers. According to one
296 cryo-EM structure of an apparently activated AMPA receptor (Meyerson et al.,
297 2014) (Fig. 1C), V666C residues should be far enough apart to accommodate
298 cross-linkers up to 19 Å in length.
299
300 To maintain the active state, we blocked desensitization with cyclothiazide
301 (CTZ, 100 μM). As shown in Fig. 4, block of desensitization produced a near-
302 universal attenuation of inhibition by bis-MTS cross-linkers, in the first minute
303 of exposure (see Suppl. Table 2 for statistics). Current inhibition for every cross-
304 linker in the presence and absence of desensitization is shown in Fig. 4B. With
305 M1M, about 15% of V666C receptors recovered from inhibition with a time
306 constant of $\tau = 7.1 \pm 1$ s, n = 4, leading to the final inhibition of 0.65 ± 0.02, n =
307 12. For M3M, the recovery was even faster with $\tau = 1.98 \pm 0.2$ s, n = 8 (grey
308 dots in Fig. 4A), with about 15% the receptors recovering and leading to the
309 final inhibition of 0.53 ± 0.03, n = 9. The fast recovery indicates that with dimer
310 separation of about 9 Å, trapped receptors were in an unstable,
311 stereochemically-strained state. We could observe trapping directly from the
312 current decay, and shorter crosslinkers acted faster (Fig. 4A and D). As in
313 desensitizing receptors, M10M took the longest to trap.
314
315 With desensitization blocked, AMPA receptors displayed a clearly distinct
316 trapping profile from that of desensitized receptors (Fig. 4C). Instead of a
317 shallow parabola, the extents of trapping active state could only be satisfactorily
318 fit with third order polynomial functions. The sharper trapping profile indicated

319 a favored LBD separation of 15 Å, greater than the optimum of desensitized
320 receptors (11 Å).

321
322 The less profound inhibition we observed in non-desensitized receptors led us
323 to investigate the possibility that M10M modifies non-desensitizing V666C
324 receptors in other ways than current amplitude reduction. We measured the
325 rate of receptor deactivation before and after the trap in M10M in the presence
326 of CTZ and found no difference (Suppl. Fig. 4 C-D, $\tau_{pre\text{-}trap}$ = 1.7 ms ± 0.2, $\tau_{post\text{-}}$
327 $_{trap}$ = 1.6 ± 0.2 ms, n = 8, P = 0.05 (paired randomisation test)). We considered
328 the possibility that non-desensitizing receptors were modified by M10M, but in
329 a way that was silent to our electrophysiological approach. We tested this
330 scenario with the following experiment: a patch with V666C receptors was first
331 trapped in M10M and CTZ; CTZ was then washed-out the patch and freely
332 desensitizing V666C receptors were exposed to M10M only (Suppl. Fig. 4A). If
333 non-desensitizing V666C receptors had been silently modified by M10M, then
334 a fraction of the receptors should have been protected resulting in the reduced
335 sensitivity to further trapping by M10M. V666C receptors initially exposed to
336 M10M in the presence of CTZ were modified to the same extent as naïve
337 receptors by M10M once CTZ was unbound (I_{peak} post-trap / I_{peak} pre-trap for
338 V666C initially trapped in CTZ: 0.23 ± 0.04, n = 6 and for V666C never trapped
339 in CTZ: 0.30 ± 0.03, n = 16, P = 0.07; Suppl. Fig. 4B). Taken together, these
340 results strongly suggest that the reduced inhibition reflected state dependent
341 protection from modification.

342

343 **Auxiliary subunits do not alter the geometry of desensitized receptors**

344 Trapping with bis-MTS cross-linkers so far indicated more conformational
345 flexibility of the LBD layer in desensitized than activated AMPA receptors.
346 However, synaptic AMPA receptors are rarely expressed alone, and are
347 instead associated with various auxiliary proteins that re-define their kinetic
348 properties (Schwenk et al., 2012; Jackson and Nicoll, 2011). We, therefore,
349 wondered if the presence of auxiliary subunits, such as Stargazin (Stg), could
350 affect conformational flexibility of AMPA receptors.

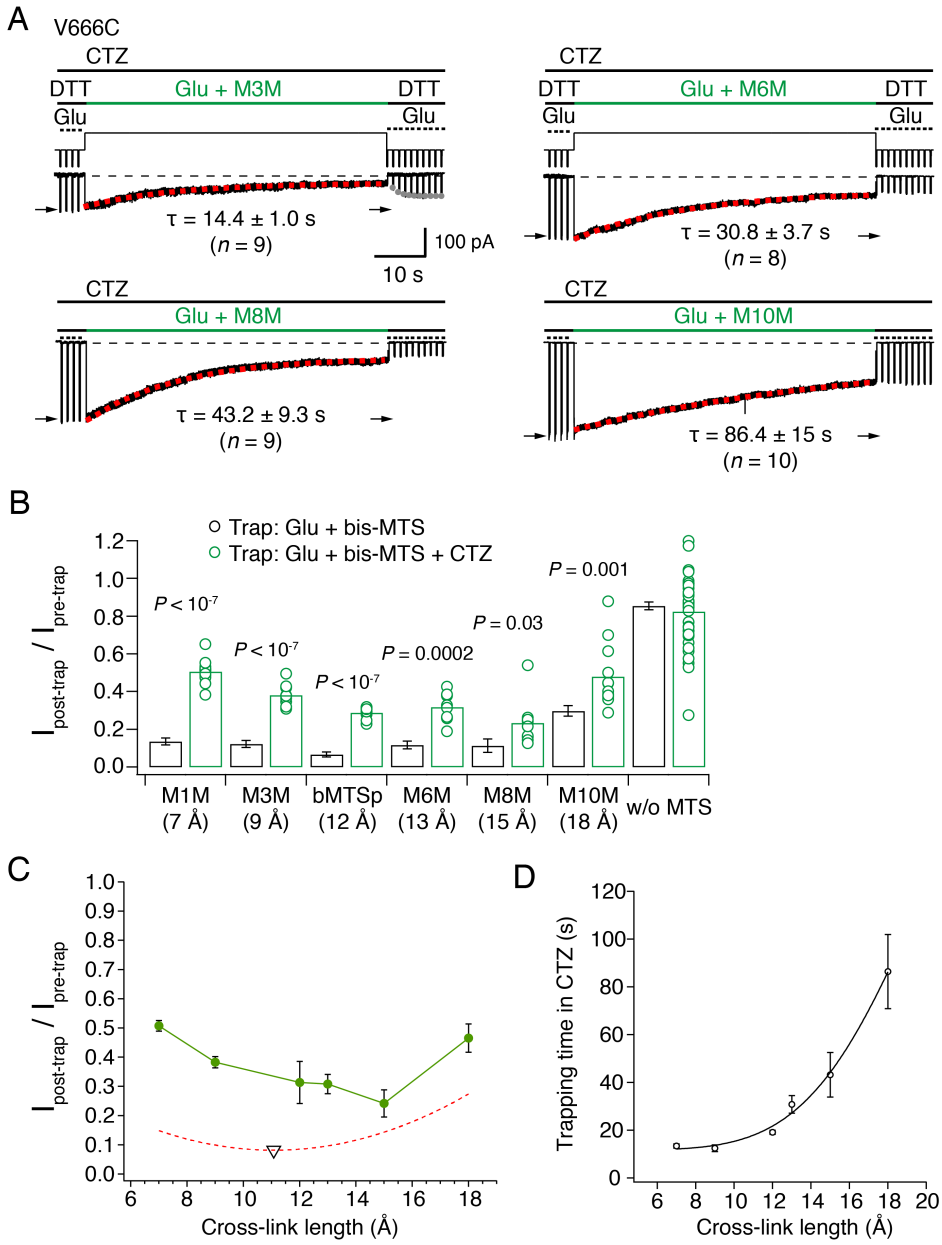

Figure 4 The active LBD layer is dilated (A) Current traces of trapping protocols on active V666C receptors. Cyclothiazide (CTZ) was included at 100 μM throughout the experiment to block desensitization. The duration of the trapping pulse shown is indicated in green. Trapping rate (τ) was determined from the monoexponential fits (red, dotted line; *n*: number of patches). For M3M, gray, dotted line indicates recovery from the trap immediately after the trap (τ = 2.0 ± 0.2 s, *n* = 8). Extent of trapping was relative to the initial pulses (arrows) (B) Summary of bis-MTS trapping (1 min) of desensitizing (black) and non-desensitizing V666C receptors (green). Desensitizing data are from Fig. 2E. *P* values compare the desensitizing and non-desensitizing condition. For *P* values comparing effects with and without bis-MTS, see Suppl. Table 2. Bis-MTS length is indicated in brackets; "w/o MTS": without MTS. (C) Trapping profile of active V666C receptors after the first minute of exposure (green). Green line merely connects the points. Fit of the trapping profile of desensitized receptors is shown as a red, dashed line for comparison. Black triangle indicates minimum of the fit at 11 Å . (D) Plot summarizing the increase of the trapping time in CTZ for V666C receptors with bis-MTS length. The solid line is a Hill equation fit to the data with no physical meaning.

366 Recently, cryo-EM structures of AMPA receptors in complex with auxiliary
367 subunits have been acquired in resting, active and desensitized states (Fig. 1B)
368 (Chen et al., 2017; Twomey et al., 2017a). These structures all predict reduced
369 separation of V666C residues when compared to receptors without auxiliary
370 proteins. For example, sulfhydryl groups of V666C residues on subunits A and
371 C are 19 Å apart in the apparent active state of isolated receptors and 15 Å in
372 activated receptors complexed with Stg (Fig. 1C). In the desensitized state, the
373 equivalent residues are 21 Å apart in homologous kainate receptors (PDB:
374 5KUF(Meyerson et al., 2016)) and 17 Å in desensitized GluA2 receptors
375 associated with GSG1L auxiliary proteins (Fig. 1C, PDB: 5VHZ (Twomey et al.,
376 2017b)). If, indeed, auxiliary subunits keep the LBD layer more compact, we
377 reasoned that their presence should also limit the effects of longer bis-MTS
378 cross-linkers.
379
380 To test this hypothesis, we repeated the trapping experiments on complexes of
381 AMPA receptors with Stg (Fig. 5). GluA2 and Stg were co-expressed and
382 association of complexes was assessed by measuring the ratio of kainate
383 current over glutamate current (KA/Glu). The relative efficacy of the partial
384 agonist kainate is known to be higher for GluA2-Stg complexes than for GluA2
385 alone, making it a good marker of GluA2-Stg association (Tomita et al., 2005;
386 Shi et al., 2009). After establishing formation of the GluA2 V666C-Stg
387 complexes in the patch, we proceeded with the trapping protocol that exposed
388 complexes to glutamate and a bis-MTS cross-linker (1 μM) for 1 minute (Fig.
389 5), as described previously. No blocker of desensitization was added and the
390 receptors were allowed to desensitize freely. Therefore the crosslinking
391 represents trapping across a mixture of active and desensitized states.
392
393 The trapping results summarized in Fig. 5C show that the presence of auxiliary
394 subunit Stg apparently protected V666C receptors from cross-linking by bis-
395 MTS. Indeed, following trapping, a robust response was preserved, and could
396 not be overcome by longer trapping intervals. This protection probably reflects
397 an exaggerated role in channel gating for B and D subunits (in principle

398 untouched by our crosslinking approach), revealed or possibly amplified by
399 Stargazin (see Discussion).
400
401 To test whether bis-MTS cross-linkers perhaps act on non-complexed V666C
402 receptors only, without affecting V666C-Stg complexes, we measured the
403 KA/Glu current ratio before and after the bis-MTS trap for a series of patches.
404 We reasoned that if only non-complexed V666C receptors were being modified,
405 the glutamate-activated current should reduce, but the kainate current (which
406 is almost entirely carried by GluA2-Stg complexes) should not. Therefore,
407 preferential trapping of non-complexed V666C mutants should lead to an
408 increase in KA/Glu ratio. As shown in Fig. 5E, the KA/Glu ratio was not affected
409 (before trap: 0.46 $\pm$ 0.03; after trap: 0.43 $\pm$ 0.02, n = 13; P = 0.2, paired
410 randomisation test), indicating V666C-Stg complexes were being modified by
411 bis-MTS cross-linkers.
412

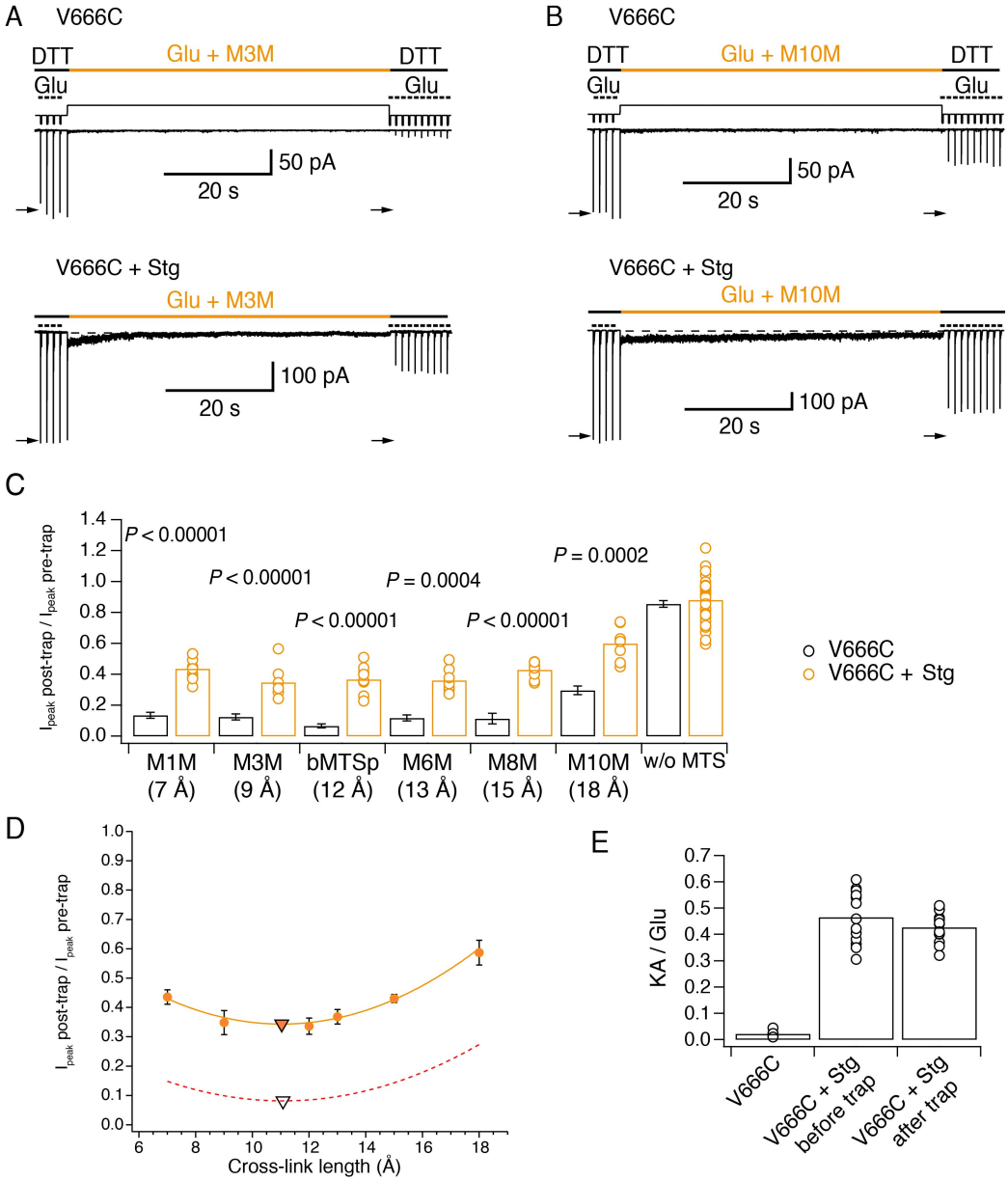

Figure 5. Stargazin attenuates effects of bis-MTS cross-linkers. (A) Current traces of V666C trapping in M3M, without (top) and with Stargazin (Stg; bottom). Legend is the same as in Fig. 2, with a trapping pulse shown here in orange. (B) Same as in (A), but for M10M. (C) Trapping effects for V666C without (black) and with Stg (orange). Post- and pre-trap peak current was determined from the control pulses (arrows in (A) and (B)). Data without Stg are the same as in Fig. 2D. Lengths of the cross-linkers are indicated in brackets and *P* values compare the effects of the respective cross-linker with and without Stg. (D) Trapping profile of desensitizing V666C+Stg complexes (data after the first minute of bis-MTS exposure). The data were fit with a parabola (orange line); the fit reaches minimum (orange triangle) at (11, 0.3). Trapping profile of desensitized receptors without Stg is shown as red, dashed line for comparison with the minimum at (11, 0.1) (black tringle). (E) The kainate/glutamate (KA/Glu) peak current ratio was determined for each patch before and after trapping with a bis-MTS (similar to the experimental design in Fig. 3A-C with 1mM KA and 10 mM Glu in 1 mM DTT). V666C + Stg KA/Glu measurements before and after trap shown here are paired recordings, pooled for various bis-MTS cross-linkers.

427 **Stargazin maintains active receptors in a compact arrangement**

428 The trapping profile of V666C-Stg complexes (orange in Fig. 5D) reflects the
429 partial protection from trapping in the presence of Stg for all cross-linker
430 lengths, but its overall shape is practically superposable onto the trapping
431 profile of desensitized V666C receptors without Stg (red, dashed line in Fig.
432 5D). Strikingly, the two curves reach their minimum at the same point of 11 Å
433 (triangles in Fig. 5D) and have identical curvature. This indistinguishable length
434 dependence indicated that the trapping of V666C-Stg complexes came
435 primarily from trapping desensitized receptors, and that the active complexes
436 of V666C-Stg might be untouched by bis-MTS cross-linkers.

437

438 To test this hypothesis, we repeated the trapping protocol in the presence of
439 CTZ, to block desensitization of V666C-Stg complexes. Two cross-linkers were
440 tested in this condition: M1M, the shortest one, and M8M, which had the
441 strongest trapping effect on active V666C receptors without Stg (Fig. 4B-C). As
442 predicted, neither bis-MTS cross-linker had any effect on activated GluA2-Stg
443 complexes ($P = 0.5$, paired recordings with and without bis-MTS) (Fig. 6). Over
444 very long exposures, M8M could induce irreversible inhibition, presumably from
445 residual desensitization. This result confirmed that partial trapping observed for
446 desensitizing V666C-Stg mainly derived from bis-MTS cross-linkers accessing
447 desensitized complexes. The most parsimonious explanation for the protection
448 is that the dimers are preferentially held in a compact arrangement that protects
449 V666C from reacting with crosslinkers. Overall, Stargazin complexes are more
450 compact than their counterparts lacking any auxiliary protein.

451

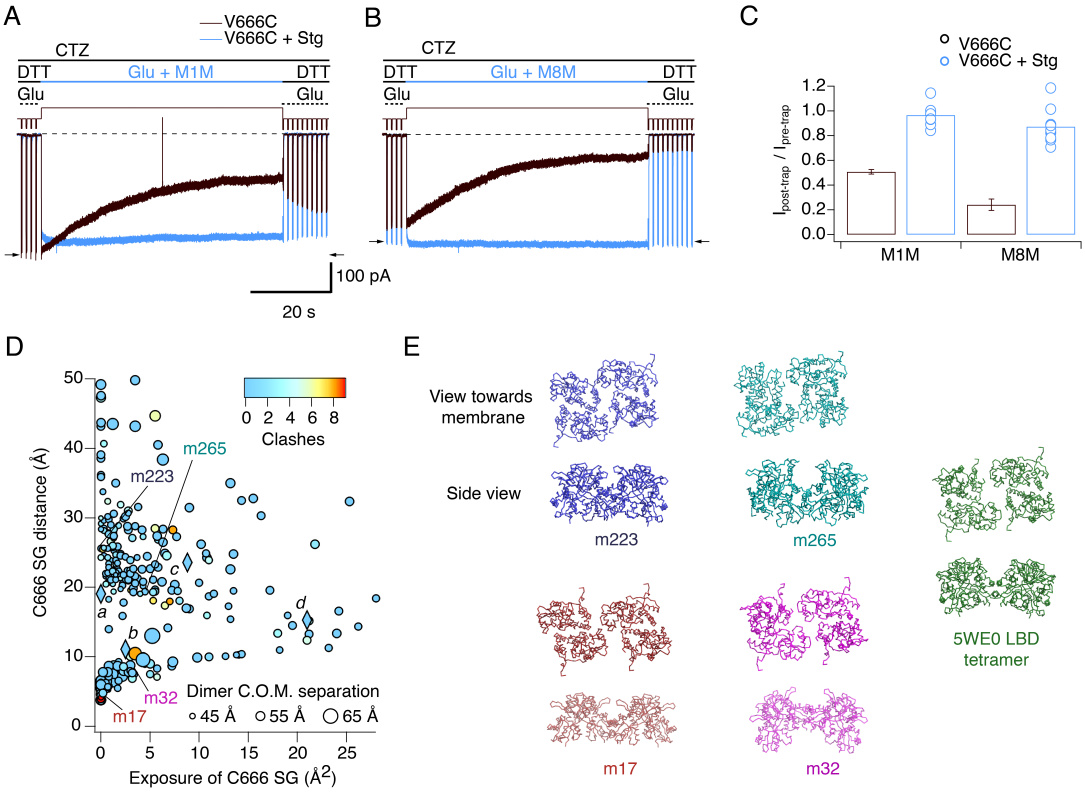

Figure 6 Stargazin blocks access to bis-MTS cross-linkers in the active state. (A) Traces showing trapping by M1M in the active state in the absence (black) and presence (blue) of Stargazin (Stg). Legend is the same as in Fig. 2, with a trapping pulse shown here in blue. Desensitization was blocked by CTZ (100 μM) present throughout the experiment. Glutamate (Glu) was 10 mM and DTT 1mM. (B) Same as in (A), but for M8M cross-linker. (C) Summary of the trapping effects for M1M and M8M in the active state in the absence (black) and presence (blue) of Stg. Pre- and post-trap current was determined from control pulses as indicated by arrows. There was no difference in effect between M1M and M8M with Stg (P = 0.1, n = 9 and 11, respectively). (D) Putative compact structures that could protect from bis MTS modification. Results of 268 runs of rigid body docking of LBD dimers against each other, to minimize Cys666 access in subunit A and mimic the protection from crosslinking. Results from known structures (5JEI, 4YU0 loose, 4YU0 tight and 5WE0, diamonds *a-d*) and generated models segregate into two classes, similar to the loose (SG-SG distance between subunits < 10 Å) and tight arrangements (SG-SG distance > 20Å, SG buried close to helix K) (Baranovic et al., 2016). The symbol size corresponds to the dimer centre of mass separation and the colour to the number of atom clashes (distance < 2.2 Å.) (E) Four models marked on the graph in panel D, and the original seed for each optimization, the glutamate bound LBD tetramer from 5WE0 full-length GluA2 structure with Stg.

470 **Discussion**

471 Technical advances in cryo-electron microscopy have revolutionized the study
472 of membrane proteins, and the supply of structural information is greater than
473 ever before. However, as the catalogue of images swells, the need to relate
474 their geometry to dynamics becomes ever more pressing. In case of AMPA
475 receptors, full-length structures in complexes with various ligands and auxiliary
476 subunits have been published. Here we have used a classical crosslinking
477 approach allied to rapid perfusion to measure distances up to 18 Å in AMPA
478 receptor extracellular domains across different functional states and in the time
479 domain.

480

481 Bis-MTS cross-linkers have been used previously to aid identification of
482 movements underlying state transitions in AMPA and NMDA receptors
483 (Armstrong et al., 2006) (Tajima et al., 2016). Here, we report effects with a
484 strong dependence on the target site, length of the cross-linker, functional state
485 of the receptor and the presence or absence of auxiliary subunits. Since most
486 bis-MTS cross-linkers are alkyl chains and hence flexible, we tested the bMTSp
487 linker that includes a rigid benzene ring, but otherwise has a very similar length
488 to M6M. The only difference we observed between these two cross-linkers was
489 with K493C mutant, with M6M blocking desensitization more effectively than
490 bMTSp, perhaps indicating an angle between the K493C side chains that was
491 more easily accommodated by the flexible chain. At other sites, rigidity had little
492 influence.

493

494 All bis-MTS cross-linkers inhibited the current, irrespective of the functional
495 state. Indeed, all inter-dimer constraints seem to be inhibitory (Plested and
496 Mayer, 2009) (Lau et al., 2013; Baranovic et al., 2016; Yelshanskaya et al.,
497 2016). Whereas the zinc and disulphide bridges, previously used to cross-link
498 LBD dimers, only form under strict geometrical requirements, the same cannot
499 be said for bis-MTS cross-linkers. The cross-linkers are flexible and therefore
500 do not restrict the trapped LBD tetramer to a single geometry. The inhibitory
501 effect of the crosslinkers is not universal – at the active intra-dimer interfaces

502 we could potentiate receptors as shown previously (Armstrong et al., 2006). It
503 appears that crosslinks between dimer pairs, or indeed any restriction between
504 the active dimers, leads to a decrease in activity.
505
506 In Fig. 7A-B, the trapping profiles of V666C receptors with the available
507 structural models of GluA2 in the equivalent condition are compared. The
508 shallow trapping profile of desensitized AMPA receptors (Fig. 2G) indicates a
509 structural ensemble of conformations broadly in agreement with multiple
510 desensitized states (Meyerson et al., 2014) (Robert and Howe, 2003)(EMDB:
511 2688). Even though the LBD dimer-dimer separation observed in the model
512 (>18 Å) was not tested with the bis-MTS cross-linker of the corresponding
513 length, extrapolation of the trapping profile indicates such conformations are
514 available to desensitized AMPA receptors. However, the longest cross-linker
515 (18 Å) was the slowest one to act on desensitized receptors, indicating that this
516 conformation, and more 'dilated' ones, are not readily available for cross-
517 linking, but slowly get populated during prolonged exposures to agonist. The
518 same trend, of the trapping time increasing with the length of the cross-linker,
519 was present in the active state. There, the most readily accessible separation
520 of V666C residues was at 15 Å (green in Fig. 7B) with 19 Å separation,
521 predicted by the structural model (PDB: 4UQ6), taking longer to populate.
522 Notably, 'dilations' of extracellular domains were also seen in antagonist-bound
523 NMDA receptors (Zhu et al., 2016).
524
525 The presence of Stg leads to universal attenuation of the cross-linking effect,
526 for all bis-MTS lengths and both functional states, desensitized and active
527 (orange and blue in Fig. 7A and B, respectively). This result seems to chime
528 with structural experiments, where the presence of Stg made the LBD layer
529 more compact. In the desensitized state, the shape of the trapping profile is the
530 same, with or without Stg (Fig. 7A), with both parabola reaching a minimum
531 point at 11 Å (triangles in Fig. 7A). This is in excellent agreement with the
532 structure of desensitized GluA2-Stg complex (PDB: 5VOV). In the active state,
533 our results deviate from the available full-length active structures. Both short

534 and long (7 or 15 Å) bis-MTS reagents failed to inhibit currents in the first minute
535 of trapping, indicating more compact LBD arrangements over this timescale
536 than obtained in the structures.
537
538 The protection from trapping in our cross-linking experiments most likely has
539 multiple origins. Although "protection" could result from a persistent long-
540 distance separation, outside the range of the crosslinkers, several observations
541 and common sense speak against this possibility. First, we previously showed
542 that active receptors (glutamate + CTZ) could be trapped by zinc bridges in
543 compact arrangements (Baranovic et al., 2016). Second, the long distance
544 must be maintained throughout the exposure, because any transit between
545 compact and dilated arrangements must pass through intermediate
546 separations, allowing crosslinkers to span the gap. Third, even the most dilated
547 structures are in the range of crosslinker lengths that we used. Fourth, the
548 mixed trapping condition for Stg-complexes in the absence of CTZ apparently
549 supports desensitized state trapping over a wide range of geometries but no
550 additional active state trapping. We reasoned that the best explanation is
551 reduced accessibility of cysteine residues during exposure to bis-MTS, perhaps
552 because the Cys666 residues are buried against other subunits or oriented
553 such that the V666C side chain makes the sulfhydryl group inaccessible for
554 cross-linking. This interpretation would mean that the active LBD tetramer is
555 even more compact than that seen in CryoEM structures with Stg(Chen et al.,
556 2017; Twomey et al., 2017a). We mined possible conformations of the LBD
557 tetramer using a coarse docking approach, allowing each active dimer to move
558 in the membrane plane, and allowing rotation of one dimer with respect to the
559 other around axes parallel and perpendicular to the active dimer interface
560 (Figure 6D and E). Interestingly, docked structures with low Cys666
561 accessibility segregated into two classes, a loose arrangement where Cys666
562 were physically close but sterically hindering each other, and a tighter
563 arrangement of the LBDs with V666C close to helix K, not unlike the structure
564 of the V666C mutant LBD bound with fluorowillardine (5JEI) (Salazar et al.,
565 2017). In that structure, additional shielding of the V666C side chain is afforded

566 by its being shielded by neighbouring structural elements. We cannot discount
567 specific, state-dependent protection from crosslinking, produced by a unique,
568 closed-cleft LBD conformation provoked by Stg in the active state, but it seems
569 to us unlikely.
570
571 No matter how avid and complete trapping is, a possible source of receptor
572 activity after trapping is the activity of free (non-crosslinked) subunits. In all our
573 experiments, subunits *A* and *C* are trapped whereas *B* and *D* are not (Fig. 7C).
574 In GluA2 receptors without Stg, even in the presence of CTZ, the activity of only
575 two subunits (e.g. *B* and *D*) produces only low conductance openings with short
576 open times (Rosenmund et al., 1998). But the presence of Stg (Coombs et al.,
577 2017) (Zhang et al., 2014) increases the current carried by receptors with one
578 or two active subunits. In our experiments, Stg had an indefatigable effect of
579 maintaining receptor activity in the limit of long exposures to bis-MTS. The
580 effect of Stg was inordinately large, with a maximum effect of the crosslinking
581 leaving approximately half the receptor activity unscathed. A simple back-of-
582 the-envelope calculation suggests this effect is larger than expected from single
583 channel recordings. The conductance from two subunits, with desensitization
584 blocked should be about 40% but with $P_{open} < 1$ (Coombs et al., 2017). This
585 result therefore provides a first estimation, albeit indirect, of the stronger effect
586 of the B and D subunits in gating. This effect is predicted because these
587 subunits have greater leverage to open the pore deriving from their more
588 peripheral location (Sobolevsky et al., 2009).
589
590 We presume that the basal compactness of the LBD layer is related to
591 observation that longer cross-linkers have slower trapping rates, indicating slow
592 adoption of 'dilated' conformations. We cannot rule out the possibility that slow
593 reaction times are somehow linked to the bis-MTS mechanism itself, but
594 alkylthiosulfonates are generally distinguished by their extremely rapid
595 reactivity in mild conditions, selectivity for cysteinyl sulfhydryl groups, general
596 reversibility upon addition of thiols such as DTT and their ability to effect
597 quantitative and complete conversion to the disulphide without applying a large

excess of reagent (Kenyon and Bruice, 1977). Our reaction rates are close to the maximum expected (10^5 $M^{-1}s^{-1}$; (Liu et al., 1997)).

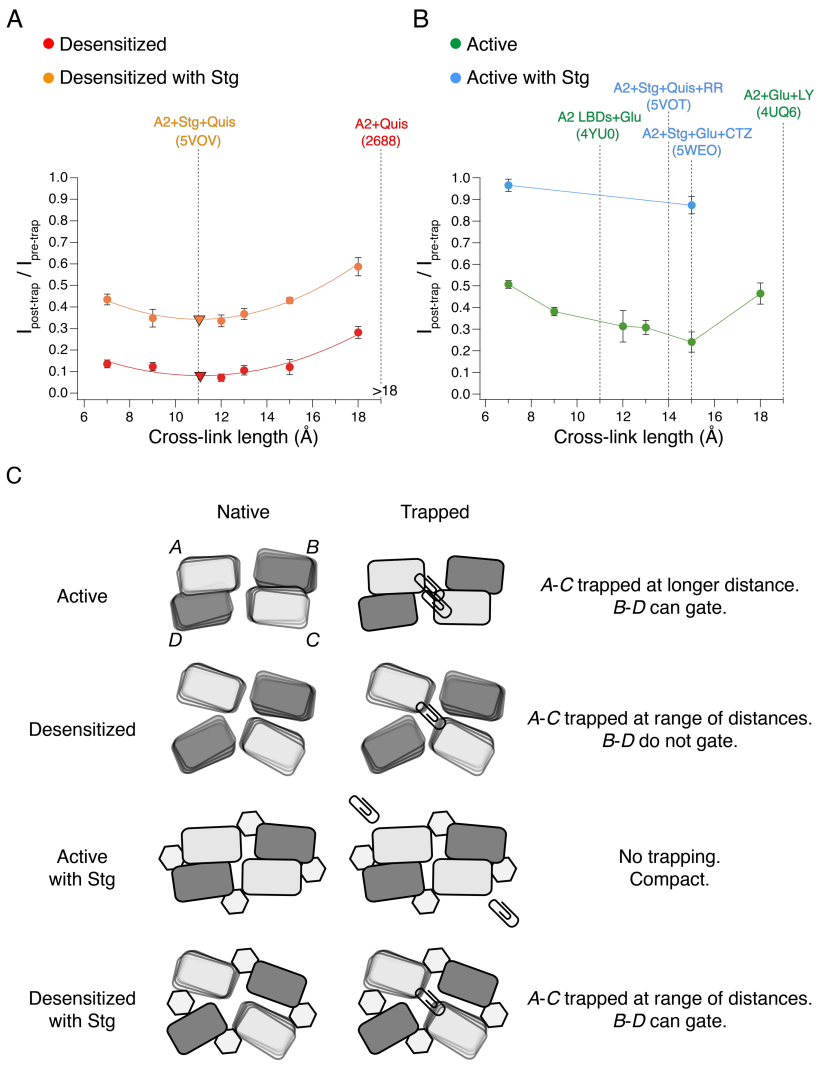

Figure 7 Comparison of structural models with V666C cross-linking profiles. (A) Trapping profiles for V666C in desensitized states, without (red) and with (orange) Stargazin (Stg). Solid lines are fit parabola, with local minima indicated as triangles. For desensitized condition without Stg, minimum is reached at (11, 0.1) and with Stg at (11, 0.3). The right handside of the x-axis is marked as >18 Å, as the resolution of the only available desensitized structure without auxiliary subunits is too low to measure residue distances. Vertical, dashed, black lines indicate V666C sulfhydryl separation in the respective structure (PDB accession codes in brackets). Names of structures are colour-coded same as the trapping profiles. (B) Same as in (A), but for active state without (green) and with (orange) Stg. 4YU0 is a structure of soluble, isolated LBDs. Quis stands for quisqualate (full agonist), RR for (R, R)-2b (Kaae et al., 2007) and LY for LY451646 (both desensitization blockers). (C) Cartoon depicting cross-linking (paperclips) of *A-C* subunits (light grey), while *B-D* subunits are left free (dark grey). 'Native' column represents apparent conformations of the LBD layer when it is not crosslinked. Muliple overlaid tiles indicate multiple available positions of an LBD.

614 Physiological activation and desensitization of AMPA receptors takes place on
615 a millisecond timescale, and we monitored this process wherever possible
616 during our experiments. Generally, the remaining current responses were not
617 altered following bis-MTS exposures. The fast gating contrasts to desensitized
618 states trapped by bis-MTS cross-linkers that are accessed after minutes-long
619 exposures to glutamate (Fig. 2F) and take tens of minutes to recover (Fig. 3).
620 Though we necessarily worked at low bis-MTS concentrations to avoid
621 confounding effects like chaining and non-specific modification, mandating slow
622 trapping, the slow recovery from trapping is striking. It seems reasonable to
623 assume that the degree of stabilization by different crosslinkers is similar, and
624 that the difference in stability comes from the states themselves. This idea is
625 supported by the cut-off that we observe – for crosslinkers longer than 10 Å,
626 crosslinking in desensitized states is irreversible over 10 minutes. In contrast,
627 AMPA receptors trapped through disulphide bridges at the same sites recover
628 in hundreds of milliseconds (Lau et al., 2013; Salazar et al., 2017). Assuming
629 that the length of the bis-MTS cross-linkers reflects level of structural
630 rearrangements and following the trend plotted in Fig. 3H, this suggests that
631 AMPA receptors exposed to brief glutamate transients at synapses are unlikely
632 to undergo extreme conformational changes, due to their complexation with
633 auxiliary subunits.
634
635 Long agonist exposures of minutes to hours are necessary in structural biology
636 experiments and could, thus, contribute to the prevalence of more 'relaxed'
637 conformations in full-length structures without auxiliary subunits (Fig. 8).
638 However, long exposures to agonists are at odds with synaptic conditions
639 where AMPA receptors see glutamate on a millisecond timescale, before it is
640 actively cleared by transporters (Clements, 1996). Furthermore, any large
641 structural rearrangements of the extracellular domains would need to be
642 accommodated by the crowded synaptic environment (High et al., 2015; Tao et
643 al., 2018) and potential presynaptic interaction partners (Saglietti et al., 2007)
644 (Elegheert et al., 2016). When in complex with auxiliary subunits, no functional
645 state of AMPA receptors necessitates large domain movements, and compact

arrangements of the extracellular layer can sustain the gating process. We conclude that extracellular domains of synaptic AMPA receptors are unlikely to undergo large structural rearrangements during synaptic transmission and instead work in a fairly compact conformational regime, unless faced with long exposures to glutamate in pathological conditions.

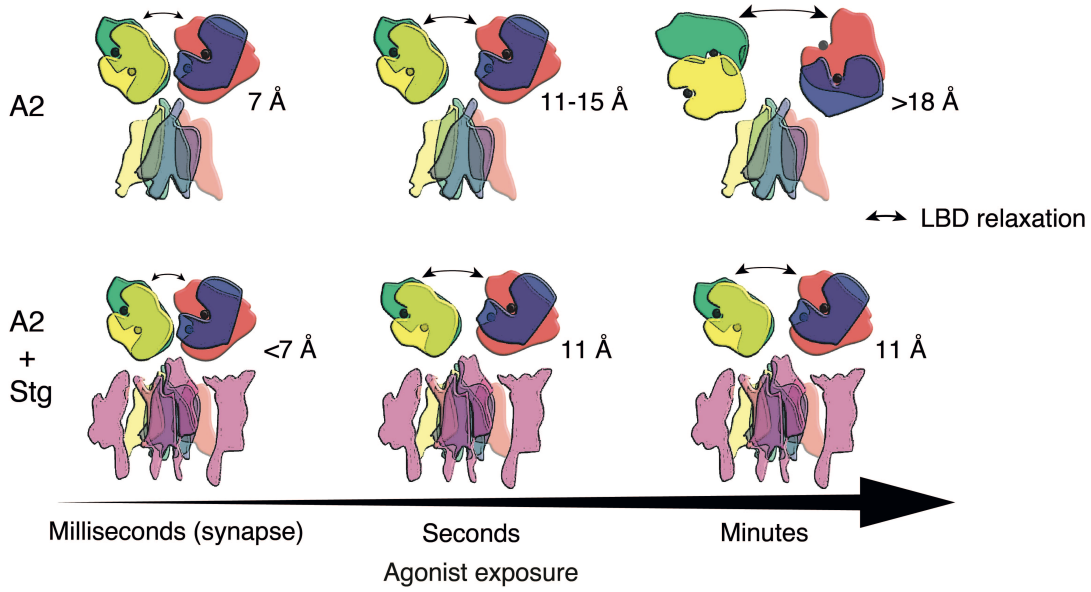

Figure 8 The presence of Stg and short agonist exposures keep the agonist-bound LBD layer compact. Schematic summarizing the bis-MTS cross-linking results. Colour-code same as in Fig. 1; ATDs are omitted. Black spheres represent bound glutamate. Upper row: in the absence of Stg, GluA2 receptors access 'dilated' LBD conformation (black arrows) upon long exposures to agonist. Bottom row: presence of Stg limits 'dilation' of the LBD layer even at longer agonist exposures.

Acknowledgements

This work was funded by the ERC Grant “Gluactive” (647895) and the NeuroCure Cluster of Excellence (DFG EXC-257). A.J.R.P. is a Heisenberg Professor of the DFG (Project number 323514590).

Author Contributions

J.B. and A.J.R.P. designed experiments, J.B. performed experiments, A.J.R.P. wrote PYTHON code and did the docking computations. J.B. and A.J.R.P. analysed data and wrote the manuscript.

670 **Experimental Procedures**

671 *Molecular Biology*

672 In all experiments, the unedited (Q586) GluA2flip version of rat A2 gene was
673 expressed from the pRK5 vector. Amino acid numbering refers to the mature
674 receptor assuming a signal peptide of 21 amino acids in length. As a marker of
675 transfection, eGFP was expressed from the same vector, downstream from an
676 internal ribosomal entry sequence (IRES). Mouse Stargazin gene (a kind gift
677 from Susumu Tomita) was expressed from a separate pRK8 vector containing
678 IRES-dsRed (Carbone and Plested, 2016). All mutations were introduced by
679 overlap PCR and confirmed by double-stranded sequencing.

680

681 *Cell Culture and Transfection*

682 GluA2 constructs were expressed transiently in HEK293 cells using calcium-
683 phosphate precipitation or PEI method as described previously (Baranovic et
684 al., 2016; Riva et al., 2017). HEK293 cells were obtained from the Leibniz
685 Forschungsinstitut DSMZ (Deutsche Sammlung von Mikroorganismen und
686 Zellkulturen GmbH, Germany) ACC no. 305, and tested negative for
687 mycoplasma. Cells were maintained in MEM Eagle medium (PAN-Biotech
688 GmbH, Aidenbach, Germany) supplemented with 10% (v/v) fetal bovine serum
689 and antibiotics (penicillin (100 U/mL) and streptomycin (0.1 mg/mL; PAN-
690 Biotech).

691

692 For transfections, 2-3 μg of DNA was transfected per 35 mm dish and cells
693 were washed after 6-8 hours. Recordings were performed 24-72 hours after the
694 transfection at room temperature. For transfections with Stargazin, Stargazin
695 DNA was co-transfected with A2 DNA at 2:1 mass ratio and after the
696 transfection, cell medium was supplemented with 40 μM NBQX to reduce
697 Stargazin-induced cytotoxicity.

698

699

700

701

702 *Solutions*

703 Chemicals were obtained from Sigma Aldrich (Munich, Germany), Abcam plc
704 (Cambridge, UK) and Hello Bio (Bristol, UK). MTS compounds were obtained
705 from Toronto Research Chemicals (North York, Canada).

706

707 The internal (pipette) solution for recordings without Stargazin contained (mM):
708 115 NaCl, 1 $MgCl_2$, 0.5 $CaCl_2$, 10 NaF, 5 Na_4BAPTA, 10 Na_2ATP, 5 HEPES,
709 titrated to pH 7.3 with NaOH. For recordings with Stargazin, the internal solution
710 was slightly modified: 120 NaCl, 0.5 $CaCl_2$, 10 NaF, 5 Na_4BAPTA, 5 HEPES
711 and 0.05 spermine, pH 7.3. The external recording solution in all experiments
712 contained (mM): 150 NaCl, 0.1 $MgCl_2$, 0.1 $CaCl_2$ and 5 HEPES, pH 7.3.
713 Different drugs were added to the external solution as needed. Glutamate was
714 always applied at 10 mM and DL-dithiothreitol (DTT) at 1 mM. Cyclothiazide
715 (CTZ) and kainate (KA) were thawed from stock solutions on the day of the
716 experiment. Final CTZ and KA concentrations in all experiments were 100 μM
717 and 1 mM, respectively.

718

719 All MTS compounds were obtained as powder. Whereas monofunctional MTS
720 reagents are known to be highly reactive and unstable in aqueous solutions
721 (Kenyon and Bruice, 1977), this information is lacking for bifunctional cross-
722 linkers used in this study. Hence, we took special care to minimize exposure of
723 bis-MTS compounds to oxidizing (aqueous) solutions (Takatsuka and Nikaido,
724 2010). The powder was dissolved in DMSO, aliquoted and kept on ice on the
725 day of the experiment. Once a stable patch recording was obtained, an aliquot
726 was dissolved in external solution to a final concentration of 1 μM and applied
727 to the patch. This way, aqueous bis-MTS solutions were on average 2-3
728 minutes old at the moment of application. Each MTS stock was tested with A2
729 wild-type receptors and A2 K493C receptors as negative and positive controls,
730 respectively. The final MTS concentration of 1 μM was chosen based on
731 previous work (Sobolevsky et al., 2003; Yelshansky et al., 2004). We avoided
732 higher concentrations of MTS compounds due to potential cross-reactivity and
733 chaining effects.

734 *Patch clamp electrophysiology*

735 Ligands and drugs were applied to outside-out patches via a custom made 4-
736 barrel glass (VitroCom, USA) mounted to a linear piezo–electric wafer
737 (PiezoMove P-601.4, PI, Germany) (Lau et al., 2013). Two barrels were
738 perfused with control solutions and the third barrel with the trapping solution,
739 as described below. All patches were voltage clamped at -40 mV unless stated
740 otherwise. Currents were low-pass filtered at 10 kHz (-3 dB cut-off, eight-pole
741 Bessel filter) using an Axopatch200B amplifier (Molecular Devices, U.S.A.) and
742 acquired with AxographX software (Axograph Scientific, Australia) at 20 kHz
743 sampling rate via Instrutech ITC-18 digitizer (HEKA, Germany).

744

745 To assess the effect of different bifunctional cross-linkers on AMPA receptors,
746 the receptors were exposed to the cross-linker (1 μM) for 1 minute. Before and
747 after this trapping exposure, the current in the patch was tested with four control
748 pulses that contained only 10 mM glutamate, without the cross-linker and in the
749 presence of DTT (1 mM) as a reducing agent (Fig. 2A-C). Four control pulses
750 before application of the cross-linker provided a measure of the patch current
751 before any exposure to the cross-linker. Accordingly, (up to thirty) control
752 pulses recorded after the MTS application, were used to assess any changes
753 in the patch current imparted by the cross-linker treatment.

754

755 For recordings of A2 receptors co-expressed with auxiliary subunit Stargazin,
756 care must be taken that A2 receptors are indeed associating with Stargazin.
757 One strategy to minimize the presence of lone V666C receptors relies on the
758 relief of spermine (polyamine) block at positive voltages imparted by
759 complexation with Stargazin (Carbone and Plested, 2016). Although we have
760 included spermine in the pipette solution and measured relieve of block for each
761 patch, we did not perform recordings at positive voltages, as the currents were
762 not stable enough during minutes-long trapping protocols. Instead, a change in
763 kainate efficacy was used as a marker of A2-Stargazin association as
764 described in the text.

765

766 *Analysis*

767 Trapping effects were quantified as the ratio of the average current after the
768 trap (determined from the post-trap control pulses 7-10, except in the case of
769 fast recovery, in which case the 2nd post-trap control pulse was used) and
770 average current before the trap (determined from the 4 pre-trap control pulses;
771 arrows in Fig. 2A-C):

$$Active\ fraction = \frac{I_{post\ trap}}{I_{pre\ trap}}$$

772

773

774 In case of desensitizing receptors, peak current was measured and in the case
775 of non-desensitizing receptors, steady-state current.

776

777 In the presence of desensitization block (i.e. CTZ), the rate of trapping was
778 described with a monoexponential fit directly to the trapping pulse (Fig. 4A) for
779 all cross-linkers. The trapping time in CTZ (τ) vs. the length of the bis-MTS
780 cross-linker (l) (Fig. 4D) was fit with a Hill equation in Igor Pro (v7.06,
781 Wavemetrics, Lake Oswego, Oregon, U.S.A.):

$$\tau(l) = \tau_{min} + \frac{\tau_{max} - \tau_{min}}{(1 + [\frac{l_{half}}{l}]^n)}$$

782
783

784 where τ_{min} and τ_{max} were the minimum and maximum time constants, n was the
785 slope and l_{half} was length of the cross-linker giving the half maximal trapping
786 time. No physical meaning was ascribed to the fitted curve. Data were weighted
787 by the standard error of the mean (SEM) for the fit. To determine the rate of
788 recovery from trapping by MTS cross-linkers, the number of post-trap control
789 pulses was increased until full recovery was attained. An envelope of post-trap
790 peak current responses was then created in Igor Pro and fit with a
791 monoexponential. This approach was possible only for faster recovery rates,
792 on the time scale of seconds, such as recovery of desensitized V666C
793 receptors from trapping with M1M (Fig. 2B and 3D) and recovery of active
794 V666C receptors from trapping with M1M and M3M (Fig. 4A). With longer bis-
795 MTS cross-linkers, the recovery time increased from seconds to minutes,

796 making direct measurements of the recovery time from post-trap control pulses
797 impractical. Instead, the experimental design was re-adjusted to allow
798 measurements of long recovery times as described in Fig. 3A-C. In brief, peak
799 current in the patch was initially recorded with 100 ms jumps into glutamate in
800 control conditions until it stabilized. Then, a trapping protocol was performed as
801 described above, with control pulses before and after the trap. After the trapping
802 protocol, the current in the patch was again monitored, for about 10 minutes,
803 with fast control jumps into glutamate in order to follow any potential recovery
804 of the peak current. In this time period, desensitized V666C receptors managed
805 to recover only from trapping by M3M (Fig. 3E and G), in which case the
806 recovery was fit with a monoexponential.

807

808 Trapping profiles (Fig. 2G and 5D) were fit with a parabola in Igor Pro:

809 $$f(x) = K_0 + K_1(x - K_2)^2$$

810

811 where K_1 defines the curvature, K_0 the minimum effect and K_2 the x value at
812 the minimum. Data points were weighted by the standard error of the mean
813 for the fit.

814

815 *Computational docking*

816 To investigate structures of the LBD tetramer that could preclude trapping by
817 blocking access to the Cys666 SG moiety, we treated each dimer as a rigid
818 body and subjected them to rotations and translations in the membrane plane.
819 Python scripts (available at github.com/aplested/cystance) were written as a
820 glue for PyMOL molecular manipulations and CCP4 functions to measure
821 geometry and exposure of the Cysteine (AREAIMOL, NCONT (Winn et al.,
822 2011)). For each run, trial arrangements that reduced Cys666 SG accessibility
823 in subunit A whilst also keeping the dimers in close proximity (with minimal
824 atom clashes) and maintaining physiologically plausible in-plane linker
825 arrangements were retained as seeds for subsequent rounds, and the step
826 size was reduced. Trial arrangements with more than 10 atom clashes (<2.2
827 Å) were rejected. No refinement was done to eliminate spurious clashes from

flexible surface residues. The optimization was ended when no further improvement was possible. Each search lasted about 5-10 minutes on a 2017 Macbook Pro.

All *P* values were determined by non–parametric randomisation test (paired or non–paired, as stated), using at least 10^5 iterations (DC-Stats suite: https://github.com/aplested/DC-Stats). Bars in graphs indicate mean and error bars SEM.

Structural models and related measurements were visualized and measured in MacPyMOL (v2.0) [The PyMOL Molecular Graphics System, Version 2.0 Schrödinger, LLC]. The length of bis-MTS cross-linkers was measured in ChemDraw Professional (PerkinElmer, U.S.A.).

842 **References**

843 Armstrong, N., Jasti, J., Beich-Frandsen, M., and Gouaux, E. (2006).
844 Measurement of conformational changes accompanying desensitization in an
845 ionotropic glutamate receptor. Cell *127*, 85-97.

846 Baranovic, J., Chebli, M., Salazar, H., Carbone, A. L., Faelber, K., Lau, A. Y.,
847 Daumke, O., and Plested, A. J. (2016). Dynamics of the Ligand Binding Domain
848 Layer during AMPA Receptor Activation. Biophys J *110*, 896-911.

849 Cais, O., Herguedas, B., Krol, K., Cull-Candy, S. G., Farrant, M., and Greger,
850 I. H. (2014). Mapping the Interaction Sites between AMPA Receptors and
851 TARPs Reveals a Role for the Receptor N-Terminal Domain in Channel Gating.
852 Cell Rep *9*, 728-740.

853 Carbone, A. L., and Plested, A. J. R. (2016). Superactivation of AMPA receptors
854 by auxiliary proteins. Nat Commun *7*, 10178.

855 Chen, L., Dürr, K. L., and Gouaux, E. (2014). X-ray structures of AMPA
856 receptor-cone snail toxin complexes illuminate activation mechanism. Science
857 *345*, 1021-1026.

858 Chen, S., Zhao, Y., Wang, Y., Shekhar, M., Tajkhorshid, E., and Gouaux, E.
859 (2017). Activation and Desensitization Mechanism of AMPA Receptor-TARP
860 Complex by Cryo-EM. Cell *170*, 1234-1246.e14.

861 Clements, J. D. (1996). Transmitter timecourse in the synaptic cleft: its role in
862 central synaptic function. Trends Neurosci *19*, 163-171.

863 Colquhoun, D., Jonas, P., and Sakmann, B. (1992). Action of brief pulses of
864 glutamate on AMPA/kainate receptors in patches from different neurones of rat
865 hippocampal slices. J Physiol *458*, 261-287.

866 Constals, A., Penn, A. C., Compans, B., Toulmé, E., Phillipat, A., Marais, S.,
867 Retailleau, N., Hafner, A.-S., Coussen, F., Hosy, E., and Choquet, D. (2015).
868 Glutamate-Induced AMPA Receptor Desensitization Increases Their Mobility

869 and Modulates Short-Term Plasticity through Unbinding from Stargazin.
870 Neuron

871 Coombs, I. D., MacLean, D. M., Jayaraman, V., Farrant, M., and Cull-Candy,
872 S. G. (2017). Dual Effects of TARP γ-2 on Glutamate Efficacy Can Account for
873 AMPA Receptor Autoinactivation. Cell Rep *20*, 1123-1135.

874 Dürr, K. L., Chen, L., Stein, R. A., De Zorzi, R., Folea, I. M., Walz, T.,
875 Mchaourab, H. S., and Gouaux, E. (2014). Structure and Dynamics of AMPA
876 Receptor GluA2 in Resting, Pre-Open, and Desensitized States. Cell *158*, 778-
877 792.

878 Elegheert, J., Kakegawa, W., Clay, J. E., Shanks, N. F., Behiels, E., Matsuda,
879 K., Kohda, K., Miura, E., Rossmann, M., Mitakidis, N., Motohashi, J., Chang, V.
880 T., Siebold, C., Greger, I. H., Nakagawa, T., Yuzaki, M., and Aricescu, A. R.
881 (2016). Structural basis for integration of GluD receptors within synaptic
882 organizer complexes. Science *353*, 295-299.

883 Geiger, J. R., Melcher, T., Koh, D. S., Sakmann, B., Seeburg, P. H., Jonas, P.,
884 and Monyer, H. (1995). Relative abundance of subunit mRNAs determines
885 gating and Ca2+ permeability of AMPA receptors in principal neurons and
886 interneurons in rat CNS. Neuron *15*, 193-204.

887 Guan, L., Murphy, F. D., and Kaback, H. R. (2002). Surface-exposed positions
888 in the transmembrane helices of the lactose permease of Escherichia coli
889 determined by intermolecular thiol cross-linking. Proc Natl Acad Sci U S A *99*,
890 3475-3480.

891 Herguedas, B., García-Nafría, J., Cais, O., Fernández-Leiro, R., Krieger, J., Ho,
892 H., and Greger, I. H. (2016). Structure and organization of heteromeric AMPA-
893 type glutamate receptors. Science

894 High, B., Cole, A. A., Chen, X., and Reese, T. S. (2015). Electron microscopic
895 tomography reveals discrete transcleft elements at excitatory and inhibitory
896 synapses. Front Synaptic Neurosci *7*, 9.

897 Jackson, A. C., and Nicoll, R. A. (2011). The Expanding Social Network of
898 Ionotropic Glutamate Receptors: TARPs and Other Transmembrane Auxiliary
899 Subunits. Neuron *70*, 178-199.

900 Kaae, B. H., Harpsøe, K., Kastrup, J. S., Sanz, A. C., Pickering, D. S., Metzler,
901 B., Clausen, R. P., Gajhede, M., Sauerberg, P., Liljefors, T., and Madsen, U.
902 (2007). Structural proof of a dimeric positive modulator bridging two identical
903 AMPA receptor-binding sites. Chem Biol *14*, 1294-1303.

904 Kenyon, G. L., and Bruice, T. W. (1977). Novel sulfhydryl reagents. Methods
905 Enzymol *47*, 407-430.

906 Lau, A. Y., Salazar, H., Blachowicz, L., Ghisi, V., Plested, A. J. R., and Roux,
907 B. (2013). A conformational intermediate in glutamate receptor activation.
908 Neuron *79*, 492-503.

909 Liu, Y., Holmgren, M., Jurman, M. E., and Yellen, G. (1997). Gated access to
910 the pore of a voltage-dependent K+ channel. Neuron *19*, 175-184.

911 Loo, T. W., and Clarke, D. M. (2001). Determining the dimensions of the drug-
912 binding domain of human P-glycoprotein using thiol cross-linking compounds
913 as molecular rulers. J Biol Chem *276*, 36877-36880.

914 Meyerson, J. R., Kumar, J., Chittori, S., Rao, P., Pierson, J., Bartesaghi, A.,
915 Mayer, M. L., and Subramaniam, S. (2014). Structural mechanism of glutamate
916 receptor activation and desensitization. Nature *514*, 328-334.

917 Meyerson, J. R., Chittori, S., Merk, A., Rao, P., Han, T. H., Serpe, M., Mayer,
918 M. L., and Subramaniam, S. (2016). Structural basis of kainate subtype
919 glutamate receptor desensitization. Nature *537*, 567-571.

920 Nakagawa, T., Cheng, Y., Ramm, E., Sheng, M., and Walz, T. (2005). Structure
921 and different conformational states of native AMPA receptor complexes. Nature
922 *433*, 545-549.

923 Plested, A. J. R., and Mayer, M. L. (2009). AMPA receptor ligand binding
924 domain mobility revealed by functional cross linking. J Neurosci *29*, 11912-
925 11923.

926 Riva, I., Eibl, C., Volkmer, R., Carbone, A. L., and Plested, A. J. (2017). Control
927 of AMPA receptor activity by the extracellular loops of auxiliary proteins. Elife
928 *6*,

929 Robert, A., and Howe, J. R. (2003). How AMPA receptor desensitization
930 depends on receptor occupancy. J Neurosci *23*, 847-858.

931 Rosenmund, C., Stern-Bach, Y., and Stevens, C. F. (1998). The tetrameric
932 structure of a glutamate receptor channel. Science *280*, 1596-1599.

933 Saglietti, L., Dequidt, C., Kamieniarz, K., Rousset, M.-C., Valnegri, P.,
934 Thoumine, O., Beretta, F., Fagni, L., Choquet, D., Sala, C., Sheng, M., and
935 Passafaro, M. (2007). Extracellular interactions between GluR2 and N-cadherin
936 in spine regulation. Neuron *54*, 461-477.

937 Salazar, H., Eibl, C., Chebli, M., and Plested, A. (2017). Mechanism of partial
938 agonism in AMPA-type glutamate receptors. Nat Commun *8*, 14327.

939 Schwenk, J., Harmel, N., Brechet, A., Zolles, G., Berkefeld, H., Müller, C. S.,
940 Bildl, W., Baehrens, D., Hüber, B., Kulik, A., Klöcker, N., Schulte, U., and
941 Fakler, B. (2012). High-resolution proteomics unravel architecture and
942 molecular diversity of native AMPA receptor complexes. Neuron *74*, 621-633.

943 Shi, Y., Lu, W., Milstein, A. D., and Nicoll, R. A. (2009). The stoichiometry of
944 AMPA receptors and TARPs varies by neuronal cell type. Neuron *62*, 633-640.

945 Sobolevsky, A. I., Rosconi, M. P., and Gouaux, E. (2009). X-ray structure,
946 symmetry and mechanism of an AMPA-subtype glutamate receptor. Nature
947 *462*, 745-756.

948 Sobolevsky, A. I., Yelshansky, M. V., and Wollmuth, L. P. (2003). Different
949 gating mechanisms in glutamate receptor and K+ channels. J Neurosci *23*,
950 7559-7568.

951 Sun, Y., Olson, R., Horning, M., Armstrong, N., Mayer, M., and Gouaux, E.
952 (2002). Mechanism of glutamate receptor desensitization. Nature *417*, 245-
953 253.

954 Tajima, N., Karakas, E., Grant, T., Simorowski, N., Diaz-Avalos, R., Grigorieff,
955 N., and Furukawa, H. (2016). Activation of NMDA receptors and the mechanism
956 of inhibition by ifenprodil. Nature

957 Takatsuka, Y., and Nikaido, H. (2010). Site-directed disulfide cross-linking to
958 probe conformational changes of a transporter during its functional cycle:
959 Escherichia coli AcrB multidrug exporter as an example. Methods Mol Biol *634*,
960 343-354.

961 Tao, C. L., Liu, Y. T., Sun, R., Zhang, B., Qi, L., Shivakoti, S., Tian, C. L., Zhang,
962 P., Lau, P. M., Zhou, Z. H., and Bi, G. Q. (2018). Differentiation and
963 Characterization of Excitatory and Inhibitory Synapses by Cryo-electron
964 Tomography and Correlative Microscopy. J Neurosci *38*, 1493-1510.

965 Taschenberger, H., and von Gersdorff, H. (2000). Fine-tuning an auditory
966 synapse for speed and fidelity: developmental changes in presynaptic
967 waveform, EPSC kinetics, and synaptic plasticity. J Neurosci *20*, 9162-9173.

968 Tomita, S., Adesnik, H., Sekiguchi, M., Zhang, W., Wada, K., Howe, J. R.,
969 Nicoll, R. A., and Bredt, D. S. (2005). Stargazin modulates AMPA receptor
970 gating and trafficking by distinct domains. Nature *435*, 1052-1058.

971 Twomey, E. C., Yelshanskaya, M. V., Grassucci, R. A., Frank, J., and
972 Sobolevsky, A. I. (2017a). Channel opening and gating mechanism in AMPA-
973 subtype glutamate receptors. Nature

974 Twomey, E. C., Yelshanskaya, M. V., Grassucci, R. A., Frank, J., and
975 Sobolevsky, A. I. (2017b). Structural Bases of Desensitization in AMPA
976 Receptor-Auxiliary Subunit Complexes. Neuron *94*, 569-580.e5.

977 Winn, M. D., Ballard, C. C., Cowtan, K. D., Dodson, E. J., Emsley, P., Evans,
978 P. R., Keegan, R. M., Krissinel, E. B., Leslie, A. G. W., McCoy, A., McNicholas,

979 S. J., Murshudov, G. N., Pannu, N. S., Potterton, E. A., Powell, H. R., Read, R.
980 J., Vagin, A., and Wilson, K. S. (2011). Overview of the CCP4 suite and current
981 developments. Acta Crystallogr D Biol Crystallogr *67*, 235-242.

982 Xu-Friedman, M. A., and Regehr, W. G. (2003). Ultrastructural contributions to
983 desensitization at cerebellar mossy fiber to granule cell synapses. J Neurosci
984 *23*, 2182-2192.

985 Yelshanskaya, M. V., Li, M., and Sobolevsky, A. I. (2014). Structure of an
986 agonist-bound ionotropic glutamate receptor. Science *345*, 1070-1074.

987 Yelshanskaya, M. V., Saotome, K., Singh, A. K., and Sobolevsky, A. I. (2016).
988 Probing Intersubunit Interfaces in AMPA-subtype Ionotropic Glutamate
989 Receptors. Sci Rep *6*, 19082.

990 Yelshansky, M. V., Sobolevsky, A. I., Jatzke, C., and Wollmuth, L. P. (2004).
991 Block of AMPA receptor desensitization by a point mutation outside the ligand-
992 binding domain. Journal of Neuroscience *24*, 4728-4736.

993 Zhang, W., Devi, S. P. S., Tomita, S., and Howe, J. R. (2014). Auxiliary proteins
994 promote modal gating of AMPA- and kainate-type glutamate receptors. Eur J
995 Neurosci *39*, 1138-1147.

996 Zhu, S., Stein, R. A., Yoshioka, C., Lee, C. H., Goehring, A., Mchaourab, H. S.,
997 and Gouaux, E. (2016). Mechanism of NMDA Receptor Inhibition and
998 Activation. Cell *165*, 704-714.

999 Zuber, B., Nikonenko, I., Klauser, P., Muller, D., and Dubochet, J. (2005). The
1000 mammalian central nervous synaptic cleft contains a high density of periodically
1001 organized complexes. Proc Natl Acad Sci U S A *102*, 19192-19197.

1002

1003 **Supplementary Material**

1004

1005 **Supplementary Table 1** Statistics of trapping desensitized A2 wild-type (WT),
1006 A665C and V666C receptors with different bis-MTS cross-linkers. The
1007 statistics in the Table accompanies data in Fig. 2D-E. The effect was
1008 measured after 1 minute of exposure to a bis-MTS.

Desensitizing receptors						
A2 WT						
	M1M	M3M	bMTSp	M6M	M8M	M10M
Active Fraction	0.89	0.84	0.78	0.88	0.85	0.81
SEM:	0.08	0.06	0.08	0.07	0.05	0.05
n:	4	11	6	6	6	8
A2 A665C						
	M1M	M3M	bMTSp	M6M	M8M	M10M
Active Fraction	-	0.45	0.48	0.53	0.48	0.40
SEM:	-	0.04	0.07	0.08	0.075	0.03
n:	-	4	7	0.01	8	5
P (vs. WT):	-	0.02	0.02	7	0.006	0.003
A2 V666C						
	M1M	M3M	bMTSp	M6M	M8M	M10M
Active Fraction	0.14	0.12	0.070	0.12	0.11	0.30
SEM:	0.02	0.02	0.01	0.02	0.03	0.03
n:	6	13	7	7	9	16
P (vs. WT):	$< 10^{-7}$	$< 10^{-7}$	$< 10^{-7}$	0.0004	0.0002	$< 10^{-7}$

1009

1010 **Supplementary Table 2** Statistics of trapping active V666C receptors with
1011 different bis-MTS cross-linkers. The statistics in the Table accompany data in
1012 Fig. 5B.

Active receptors							
A2 V666C							
	M1M	M3M	bMTSp	M6M	M8M	M10M	w/o MTS
Active Fraction	0.51	0.38	0.29	0.32	0.23	0.48	0.82
SEM:	0.02	0.02	0.01	0.03	0.04	0.05	0.03
n:	12	9	9	8	9	12	38
P (vs. w/o MTS):	$< 10^{-7}$	$< 10^{-7}$	$< 10^{-7}$	$< 10^{-7}$	$< 10^{-7}$	$< 10^{-7}$	

1013

1014

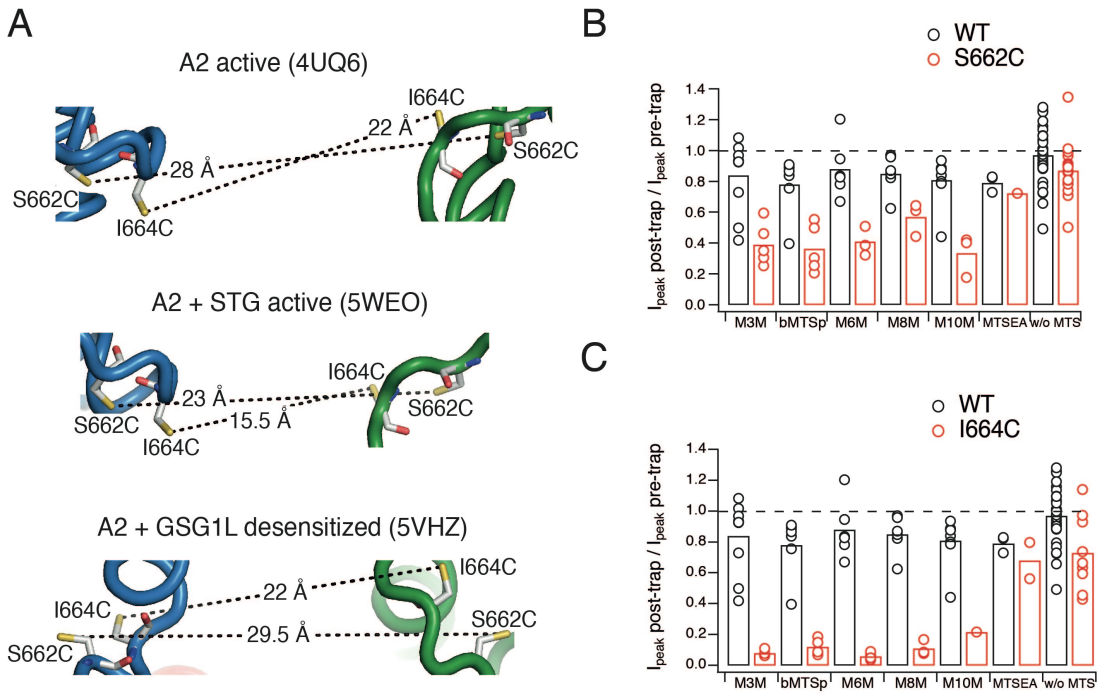

1015

1016 **Supplementary Figure 1 Effects of bis-MTS cross-linkers on A2 S662C**
1017 **and A2 I664C mutants.** (A) Distances between sulfhydryl groups of S662C
1018 and I664C residues in the respective full-length cryo-EM structures (PDB
1019 accession codes in capitals). Colour-coding as in Fig. 1. (B) Lenghts and
1020 structures of MTS compounds used to probe S662C and I664C distances in
1021 agonist-bound states. (C) Summary of trapping effects for cross-linkers M3M-
1022 M10M for S662C mutant compared with WT. WT data are the same as in Fig.
1023 2D-E. Trapping effect was measured as a ratio of the peak current post and
1024 pre-trap as described in Fig. 2. Dashed line indicates no effect. (D) Same as in
1025 (C), but for I664C mutant.

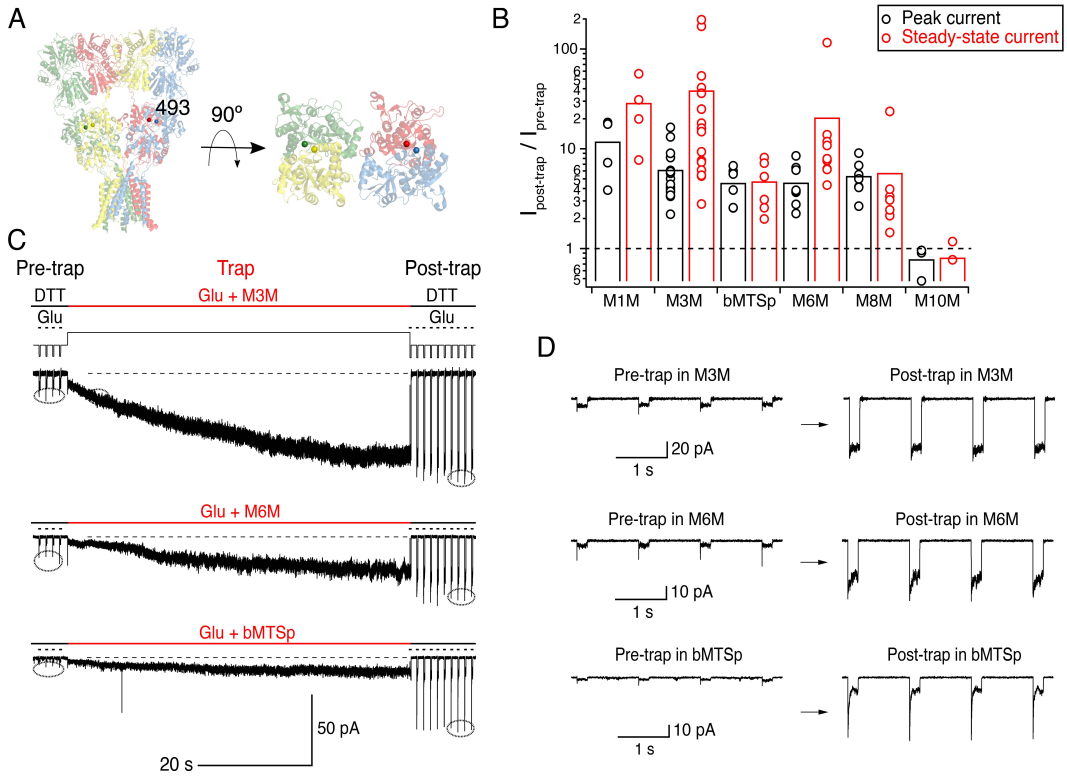

Supplementary Figure 2 Bis-MTS cross-linkers potentiate A2 K493C currents by accessing intra-dimer space. (A) Position of the K493C mutant in a full-length A2 receptor (PDB: 3KG). Subunits are colour-coded as in Fig. 1 and Cα atoms of K493C are shown as spheres. Top down view of the LBDs shows intra-dimer position of the mutation. (B) Effects of bis-MTS cross-linkers M1M-M10M on peak currents (black) and steady-state currents (red) of K493C mutant. Trapping effects are shown as a ratio of averaged post-trap over averaged pre-trap currents (encircled in (C)). Dashed line indicates no effect. (C) Current traces of A2 K493C receptors during trapping with various bis-MTS cross-linkers. Legend is the same as in Fig. 2A-C. Baseline is indicated as a black, dashed line at the bottom of each trace. Note current increase during the cross-linker application (thick, red line). (D) Zooms of encircled pre- and post-trap control pulses from traces in (C).

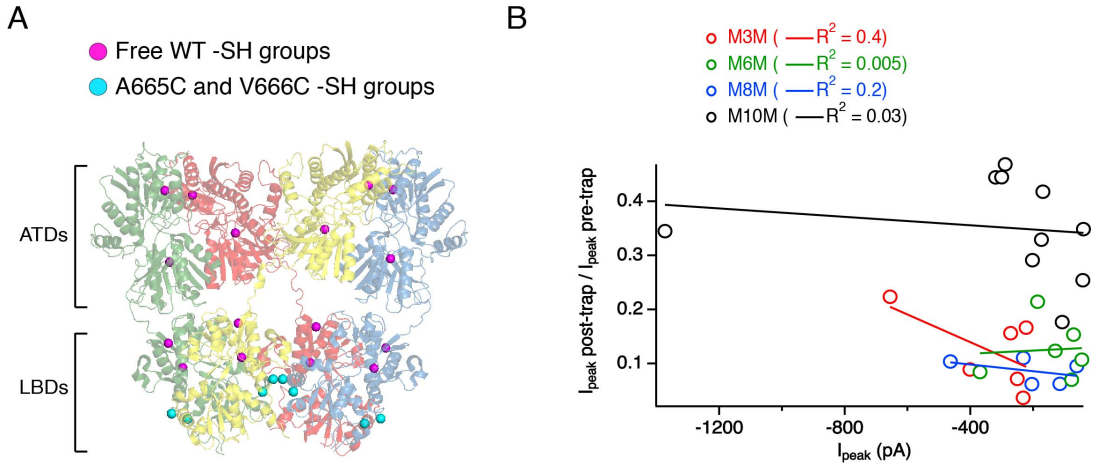

Supplementary figure 3 Bis-MTS compounds do not form inter-receptor cross-links. (A) Extracellular domains of an A2 receptor (subunits colour-coded as in Fig. 1), with S atoms of wild-type, free cysteines shown as magenta spheres and of A665C and V666C mutants as cyan spheres. (B) Plot summarizing size of the trapping effect vs. absolute peak current in the patch for M3M (red), M6M (green), M8M (blue) and M10M (black) cross-linkers. Solid lines are linear regression fits with the resulting R^2 indicated in brackets.

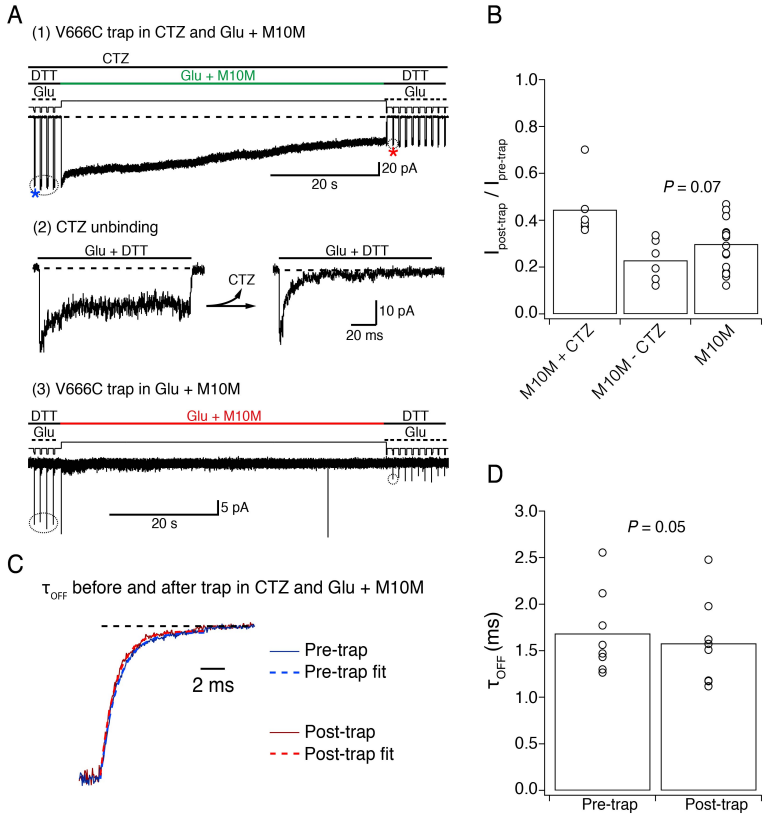

Supplementary Figure 4 No silent modification of active V666C receptors. (A) To check whether M10M modifies active V666C receptors silently, a patch containing V666C receptors was first exposed to Glu (10 mM) and M10M (1 μM) in CTZ (100 μM) to block desensitization as shown in (1). Colours are as in Fig. 2 and 4. The patch was then exposed to short (100 ms) jumps into 10 mM Glu (in reducing conditions), until CTZ unbound (2). Freely desensitizing receptors in the same patch were then exposed again to M10M and glutamate, without CTZ (3). (B) Summary of effects on V666C receptors in active state (M10M+CTZ) and after CTZ unbinding (M10M-CTZ) (paired recordings). For comparison, the trapping of patches that were never treated with CTZ (M10M) is also plotted. Pre- and post-trap current amplitudes were measured from ringed regions in (A). *P* value compares patches from which CTZ unbound and patches that were never treated with CTZ. (C) Time constant of deactivation (τ_{OFF}) was measured for active V666C receptors before (blue) and after (red) 1 min trap in M10M (from control pulses as indicated with a blue and red star in (A-1)). Normalized current decays were fit with a monoexponential. (D) Summary of τ_{OFF} as determined in (C).